WIRE BOOM DEPLOYMENT DYNAMICS AND CONTROL SYSTEM MODEL FOR SMALL SATELLITES

by

Prashant Morbhat

A report submitted in partial fulfillment
of the requirements for the degree

of

MASTER OF SCIENCE

in

Electrical Engineering

Approved:

Dr. Charles M. Swenson Major Professor	Dr. R. Rees Fullmer Committee Member

Dr. YangQuan Chen
Committee Member

UTAH STATE UNIVERSITY
Logan, Utah

2012

Abstract

Wire Boom Deployment Dynamics and Control System Model for Small Satellites

by

Prashant Morbhat, Master of Science

Utah State University, 2012

Major Professor: Dr. Charles M. Swenson
Department: Electrical and Computer Engineering

Small spacecrafts are extensively used to study space weather in the ionosphere extending from 85 km to 600 km. In this region of increased drag, small spacecrafts have much longer life span compared to their counterparts. Small form factor, along with the use of advanced sensors, make these spacecrafts highly favorable for carrying out the geospace and atmospheric research missions. In order to observe the electric field in space, the electric potential between various spatial points is needed to be measured. For this cause, sensors are deployed several meters apart in space environment. These sensors are attached to the spacecraft by wire booms. During the sensor deployment, free energy is released in the system. To avoid undesirable oscillations in the wire booms and spacecraft coning, the deployment is to be carried out with a constant rate. This research attempts to model the dynamics involved in deploying the wire booms from the spacecraft. Two models are presented in this report. The first model is a simple model where the deflection of the wire booms, as well as the mass of the boom wires, is neglected. The differential equations of motion from this model are used to design control system for deploying wire booms with a given profile. The report also shows if the designed control system is able to meet the deployment scheme and the safety requirements. The second model includes the in-plane

deflection of the wire booms. This model is used to observe the effects of deployment scheme on the in-plane oscillations of the wire booms.

(75 pages)

Public Abstract

Wire Boom Deployment Dynamics and Control System Model for Small Satellites

by

Prashant Morbhat, Master of Science

Utah State University, 2012

Major Professor: Dr. Charles M. Swenson
Department: Electrical and Computer Engineering

Small satellites play an important role in observing the space environment. In order to make electric field measurements, sensors need to be deployed many meters apart in the space environment. The sensor deployment disturbs energy in the system. To avoid coning of the spacecraft body and oscillations of the wire booms, it is important to carry out stable wire boom deployment. This report documents the methods of depicting the dynamics involved in the deployment of the wire booms from small spacecraft. The equations of motion are used to design wire boom deployment control systems for small satellites and sub-orbital payloads. An advanced model is also developed to study the in-plane oscillations occurring while deployment of the electric field sensor takes place. It also includes modeling viscous damping and wire boom spring effects on the magnitude of in-plane oscillations.

Acknowledgments

I would like to thank Dr. Charles M. Swenson for giving me an opportunity to work on this exciting project under his expert guidance. His vast experience and knowledge of spacecraft systems has always motivated and inspired me to take up the challenges involved in this work. I am highly grateful to Dr. R. Rees Fullmer for providing insights in the modeling and control system design, and Dr. YangQuan Chen for his initial help in solving differential equations in Simulink and teaching a course involving linear quadratic regulator used in this project. I appreciate the support from Bryan Bingham and DICE team in the Space Dynamics Lab. I also thank the staff of the Electrical and Computer Engineering Department, Utah State University, for their support.

Prashant Morbhat

Contents

List of Tables

List of Figures

Chapter 1

Introduction

1.1 CubeSats

Satellites play a pivotal role in carrying out space research missions. Missions dedicated to understanding the Earth's climate and environment, the Sun and its interaction with the Earth, the nature of bodies in the solar system, and space observations for exploring the universe all depend on satellites to accomplish the goals. Projects involving large satellites are so expensive that the actual access to space becomes limited. Development of large satellites require higher infrastructure, and once built, these satellites need expensive launch vehicles to lift their heavy masses into space. This increases the cost of space-based research activity and consequently decreasing the probability that it will occur. The question naturally arises whether small satellites can be constructed to effectively carry out space research, with reduced development and launch costs.

Emerging technologies based on Very-large-scale Integration (VLSI) and Microelectromechanical Systems (MEMS) and driven by the consumer portable electronics market have made it possible to construct highly capable devices like smart cell phones and hand-held computers. These technologies enable the development of sophisticated satellites that have the restrictions of small mass, power, and volume. The community refers to these satellites as "Nano-Satellites" or "Pico-Satellites." The commonly used classification of small satellites with reference to their mass can be made as given in the Table 1.1. A prime example of such satellites is the CubeSat initiated in 1999 by Stanford University and The California Polytechnic State University (Cal Poly) [1]. The essence of the CubeSat is to develop a standard size and volume container for carrying nano-satellite into space that can be attached to any launch vehicle without impacting the primary mission. The secondary payload's ride into space is low cost and is therefore expected to be available more often.

The original motivation for the CubeSat was to promote research and development in space engineering at the education level. The resulting CubeSat standard is becoming more and more popular because of reduced time and costs of satellite development. CubeSats enable more access to space which is an encouraging sign for the community dedicated to space research missions.

CubeSats can be further classified based on their form factor. A CubeSat with 1U form factor (meaning one unit) refers to structural dimension of 10x10x10 cm. A 1U CubeSat generally weighs around 1 kg. Other commonly used form factors for CubeSats are 1.5U (10x10x15 cm), 2U (10x10x20 cm), and 3U (10x10x30 cm). Since CubeSats are all 10x10 cm in cross-section (regardless of height) they can all be launched and deployed using a common deployment systems with minimal alteration between missions. CubeSats are currently being developed in many countries and at a variety of educational institutions because they provide easy access to space. Table 1.2 presents CubeSats applications, organized with respect to mission type, that have been developed by various universities across the world.

In the United States the National Science Foundation has the CubeSat-based Science Missions for Space Weather and Atmospheric Research program which aims to support the development, construction, launch, operation, and data analysis of small satellite science missions to advance space weather and atmospheric research [2]. Started in 2008 within the Division of Atmospheric and Geospace Sciences, this program has funded eight CubeSat-based projects for space weather research. Table 1.3 gives a brief summary of these NSF funded projects.

One of the compelling applications of the CubeSat is the deployment of large numbers

Table 1.1: Satellite classification.

Class of Satellite	Mass (Kg)
Small Satellite	500-1000
Mini-Satellite	100-500
Micro-Satellite	10-100
Nano-Satellite	Less than 10
Pico-Satellite	Less than 2

Table 1.2: List of CubeSats under different mission objectives.

Objective	CubeSat/s	University(ies)/Institution(s)	Country
CubeSat Technology development and demonstration	AAU CubeSat	Aalborg University	Denmark
	CanX-1	University of Toronto	Canada
	AeroCube	Aerospace Corporation	USA
	CUTE-1	Tokyo Institute of Technology	Japan
	SRMSAT	Sri Ramaswamy Memorial University	India
	JUGNU	Indian Institute of Technology Kanpur	India
Biological Science Payload	GeneSat	NASA Ames Research Centre	USA
	PharmaSat	NASA Ames Research Centre	USA
Earth Observation	QuakeSat	Stanford University	USA
	PLUME	University of Leicester	UK
	SwissCube	Ecole Polytechnique Federale de Lausanne	Switzerland
Space Tether	MAST	Tethers Unlimited, Inc. and Stanford University	USA

of CubeSats in a LEO constellation missions to address fundamental questions on space weather or to provide multipoint monitoring capability of Earth space.

1.2 Need of Electric Field Probes in Space Weather Research

Space weather research involves understanding the motion or winds of the thin gasses in the upper atmosphere of the Earth. Electric field measurements in the Earth's ionosphere are one way of observing this motion because any bulk motion of the ionospheric plasma is accompanied by an electric field. An instrument called Electric Field double Probe (EFP) is commonly used to carry out these electric field measurements in the space environment. It consists of a pair of conducting spheres immersed in the ionospheric plasma and separated by several meters distance. Previous mission have used ridged booms or have attached sensors at the ends of the wire booms on spinning spacecraft. Use of wire boom offers an ultra-lightweight design for long separation distances between EFP sensors [3]. The instantaneous potential difference between the conducting spheres attached at the ends of the wire booms is used to measure the component of electric field vector along the direction

Table 1.3: List of NSF funded projects.

Mission	Objective	University/Institution(s)	CubeSat
RAX	Measure small scale plasma density irregularities in the ionosphere.	University of Michigan and SRI International	3U CubeSat
Firefly	Explore Causal links between ground lighting and terrestrial γ-ray flashes.	Siena College and NASA Goddard Space Flight Center	3U CubeSat
FIREBIRD	Investigate size, persistence, and energy dependence of relativistic electron bursts from inner radiation belts.	University of New Hampshire and Montana State University	Two 1.5U CubeSats
DICE	Measure ionosphere density and electric field variability with the formation of geomagnetic storm.	Utah State University and ASTRA	Two 1.5U CubeSats
CINEMA	Map strong geomagnetic currents and energetic neutral atoms associate with storm time precipitation.	UC Berkeley(lead), Imperial College London, NASA Ames, Kyung Hee University	3U CubeSat
CSSWE	Measure energetics of solar produced relativistic electrons and protons during periods of intense solar flare activity.	University of Colorado at Boulder	3U CubeSat
CADRE	Measure density and composition of perturbed thermosphere using a novel sensor.	University of Michigan	1.5U CubeSat
EXOCUBE	Measure density of select species of neutral and ionized atoms in uppermost levels of the Earth's atmosphere.	University of Wisconsin, Cal Poly, and Scientific Solutions Inc.	3U CubeSat

of the boom [4]. It is based on a principle that the electric field strength at a point is equal to the negative gradient of the electric field potential.

Wire boom deployment systems have been used on several spacecraft missions in the past, but they all have fundamental similarities [5]. The systems provide a mechanism to deploy weighted sensors at the ends of flexible wires from spinning spacecraft. They basically differ in the length of the wire booms used and the mechanism adopted to deploy them. For example the electric field Instrument for THEMIS [6] and the FAST Satellite [7] made use of motors within the wire boom mechanism to actively control the deployment of the sensors. Similar deployment is being adopted for BepiColombo mission to the magnetosphere of Mercury to deploy its MEFISTO-S and WPT sensors to a length of 15 meters [8,9]. Sounding rocket missions have also made use of wire boom systems. Cornell University has developed the SIERRA wire boom system [10]. This system is similar to the yo-yo de-spin system that is used on sounding rockets that consists of a wire wrapped around the body of the rocket with a weight that when released slows the spin rate of the vehicle. The SIERRA system uses a rotary damper to avoid wire re-wrap around the spacecraft after the booms have been deployed yo-yo style from the sounding rocket.

The Utah State University's Space Dynamics Lab has two space weather research missions, the Dynamic Ionosphere CubeSat Experiment (DICE) and the Auroral Spatial Structures Probe (ASSP), that make use of wire booms to deploy electric field sensors to the ionosphere. DICE consists of two CubeSats with 5 meter wire booms and ASSP consists of six CubeSat sized payloads with 2 meter wire booms. This report will examine the dynamics involved in the stable deployment of wire boom systems from CubeSats used in DICE and sub-orbital payloads to be used in ASSP. In the next sections a description of DICE and ASSP missions along with their wire boom systems.

1.3 DICE Mission

The Dynamic Ionosphere CubeSat Experiment (DICE) mission was selected and funded by the National Science Foundation in October 2009 in response to a cooperative proposal from Utah State University's Space Dynamics Laboratory (USU/SDL), ASTRA Inc., and

Embry Riddle University. DICE is one of several missions developed under NSF's CubeSat-based Science Mission for Space Weather and Atmospheric Research program. Variations in the ionosphere's plasma density affects radio frequency based systems like communication systems, surveillance, and navigation systems on Earth and in space. Therefore, it becomes highly important to conduct studies on geomagnetic storm enhanced density features that occur in the Earth's ionosphere. DICE mission is headed to investigate the relationship between penetration electric fields and the formation and evolution of SED. DICE consists of the two CubeSats which are identical in design and function.

Students working with professionals at the Utah State University Space Dynamics Laboratory spearheaded the design, fabrication, and testing of the CubeSats. The launch of DICE occurred on October 29th, 2011, from Vandenberg Air Force Base in California at 2:48 a.m. local time. Both DICE spacecraft were inserted jointly into orbit from a P-POD carried on Delta II rocket for the Suomi National Polar-orbiting Partnership spacecraft (NPP). The DICE CubeSats will be aligned with the Earth's geodetic axis and spun up for stabilization. After sufficient time has elapsed to ensure safe inter-spacecraft separation, the wire booms of the EFP will be deployed using a novel miniature wire booms deployment system that involves controlled rate of wire boom deployment.

1.3.1 Overview of DICE CubeSat's Systems

Each DICE CubeSat conforms to a 1.5U form factor (10x10x15 cm) and can be roughly divided into payload, electronics, communication, and attitude control sub-systems.Electrical power is provided by solar panels attached to the outer faces of the CubeSat.When CubeSat is in eclipse, power stored ina high energy density lithium polymer battery will be used which afterwards get recharged through the solar panels. On board computing is provided by a Pumpkin FM430 flight control module containing a Texas Instruments MPS430 microcontroller. Communication is provided by a half-duplex UHF Cadet-U modem developed by L3 Communications for a 2.6 Mbit/s downlink (465 MHz) and 19.2 kbit/s uplink (450 MHz) [11]. The attitude control is provided by the torque coils. Attitude determination and navigation system consists of the sun sensors, a magnetometer, horizon sensor, MEMS

gyros, and a miniature GPS receiver. The DICE CubeSat's systems are shown in Figure 1.1.

Each CubeSat has three science instruments, a Langmuir Probe (DCP) to measure *in-situ* ionospheric plasma densities, an Electric Field Probe (EFP) to measure DC and AC electric fields, and a Three Axis Magnetometer (TAM) to measure field-aligned currents. The four EFP booms each extend 5 m from the spacecraft with spheres on the ends of the booms.

1.3.2 Wire Boom Deployment System for DICE

The miniature wire boom deployment system used in DICE consists of the four electric field probes, the corner probe mounts, the spool, the motorized braking mechanism. The whole system is shown in Figure 1.2. The four probe mounts are located on each corner of the deck plate (shown in red). The spool is located in the center of the deck plate and the brake assembly is located on the bottom of the deck plate. The deck plate also serves as an interface between the wire boom deployment system and the science electronics.

The spool assembly plays an important role in the deployment of the wire booms from the CubeSat. When the centrifugal force on the EFP's becomes sufficient to overcome the static friction present in the wire boom deployment system, the wire booms deploy, and the outer spool rotates in a direction opposite to that of the inner spool and the CubeSat [12]. Figure 1.2 also illustrates the motion of the spool assembly during the deployment of the wire booms. In order to make sure that the deployment of the wire booms is stable, it becomes necessary to control the rate at which the wire booms extend from the spool sub system. This can be accomplished using a breaking mechanism which consists of a small piezoelectric squiggle motor. The use of squiggle motor instead of a dc motor keeps the system free from electromagnetic interference. The squiggle motor acts as an actuator on a lever arm present underside of the deck plate. The motor steps forward to apply force on a lever arm (as shown in Figure 1.3), which rotates a brake spool present in the spool assembly. When the brake spool rotates, the string attached about the spool gets constricted, applying friction force to oppose the relative motion of the outer spool with respect to inner spool rigidly attached to the CubeSat body.

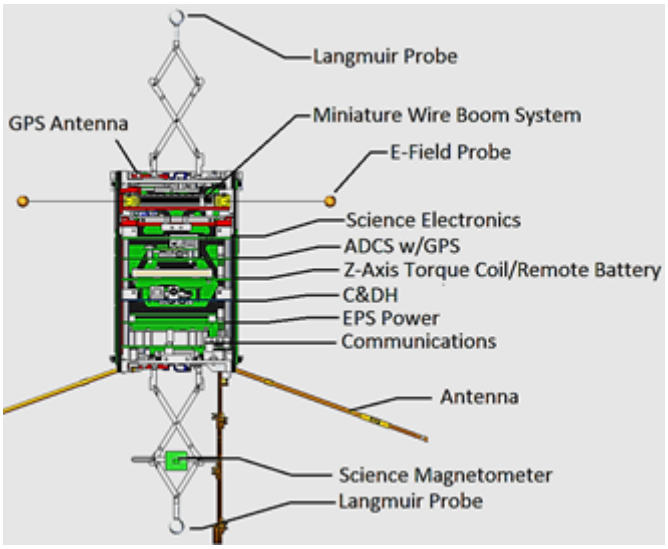

Fig. 1.1: The DICE spacecraft with electric field booms in partial deployment.

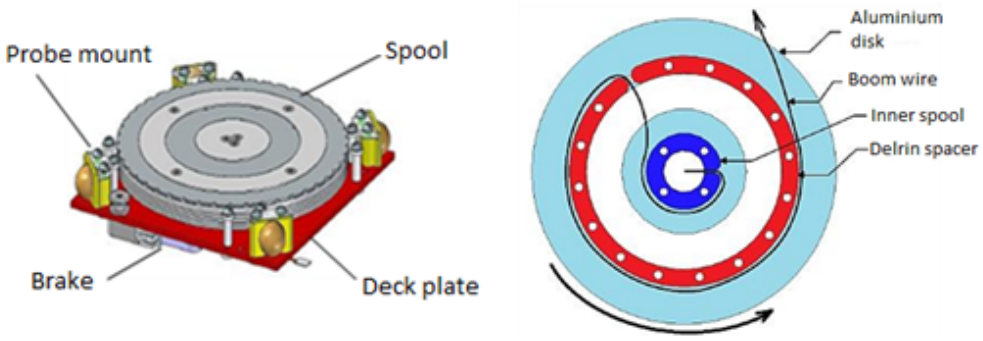

Fig. 1.2: The miniature wire boom system and rotational motion of spool.

The breaking mechanism provides an active control on the rate of boom deployment, without using any form of DC motor which is a potential source of highly undesirable noise due to electromagnetic interference. In order to sense the deployment rate, an optical encoder ring is used in the wire boom deployment control system.

1.4 Auroral Spatial Structures Probe

The Auroral Spatial Structures Probe is the next mission proposed to be conducted in collaboration between The Utah State University Space Dynamics Laboratory, ASTRA, and the University of Alaska Fairbanks. The mission falls under NASA sub-orbital science program. The objective of this mission is to study the evolution of the high-latitude electric fields during geometrically disturbed conditions, and the contributions of small-scale turbulent electric fields to the larger-scale electro-dynamical processes. The rocket will be launched out of the Poker Flat Range in the January-February 2014 time frame to an altitude of approximately 700 km towards the magnetic pole. The mission will make use of a constellation of small payloads that separate relative to each other throughout the rocket flight. Each sub-payload will carry a crossed pair of double-probe sensors to measure *in-situ* electric fields, a 3-axis magnetometer, and a GPS receiver. The data obtained at the different spatial locations and baselines (each pair of sub-payloads defining a baseline) will be used to develop models for the spatial and temporal distribution of E-fields and their correlations during auroral storms.

1.4.1 ASSP Payloads

ASSP mission consists of a main (rocket section) payload and six sub-payloads. The main payload (shown in Figure 1.4) consists of set of forward and aft air-spring ejection mechanisms along with two sets of E-field booms. A plasma impedance probe and DC Langmuir probe will be mounted along the spin axis under the nose cone to observe electron density along the rocket trajectory. The main payload will make use of an attitude control system for two maneuvers to point the payload in the proper direction for simultaneous, fore and aft, ejection of sub-payloads by air springs. Each sub-payload will be spun up to

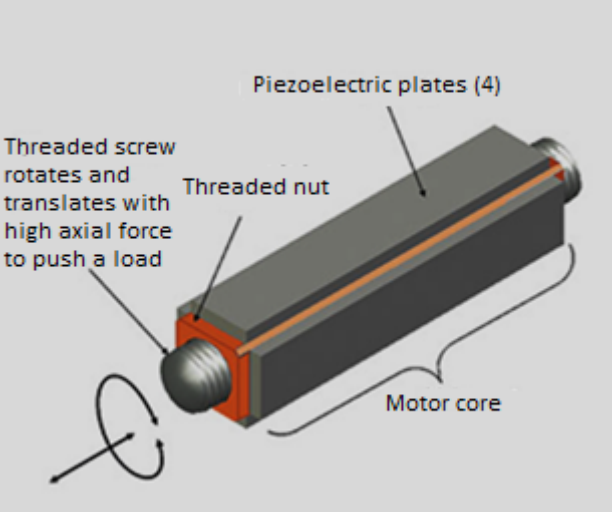

Fig. 1.3: Illustration of squiggle motor actuation.

approximately 2 Hz prior to ejection from the main payload.

The ASSP sub payloads will be constructed from systems developed the DICE mission (shown in Figure 1.1). The ASSP sub payloads, shown in Figure 1.5, will not include the C&DH, ADCS, solar panels, and power control systems as these are not needed for a sub-orbital payload. The C&DH system will be replaced with a standard telemetry formatter and transmitter (S-band frequencies) for compatibility with the poker flat range. Each sub-payload will directly telemeter its data to the ground. The wire boom system is located at the center of the payload and deploys four sensors through ports in the skin of the sub-payload to a length of 2 meters. A magnetometer is deployed at the end of a short 10 cm boom.

1.4.2 Mission Sequence and Deployment

The sounding rocket carrying the ASSP payloads will be launched to a high altitude (˜700 km apogee) along the magnetic meridian. The high altitude launch is required to provide sufficient time for the sub-payloads to separate and deploy from the main payload. The constellation will be created by ejecting four of the sub payloads fore and aft along track and two in the cross track direction. Four of the sub-payloads are ejected at 50 m/s at 90 degrees to each other in the plane perpendicular to the velocity vector of the main

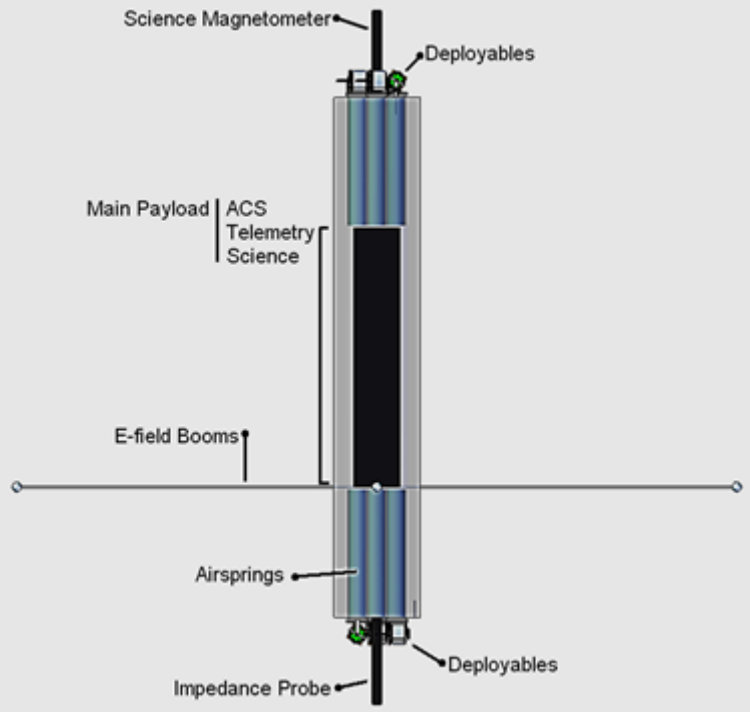

Fig. 1.4: Main payload showing the fore and aft sub-payloads and E-field booms.

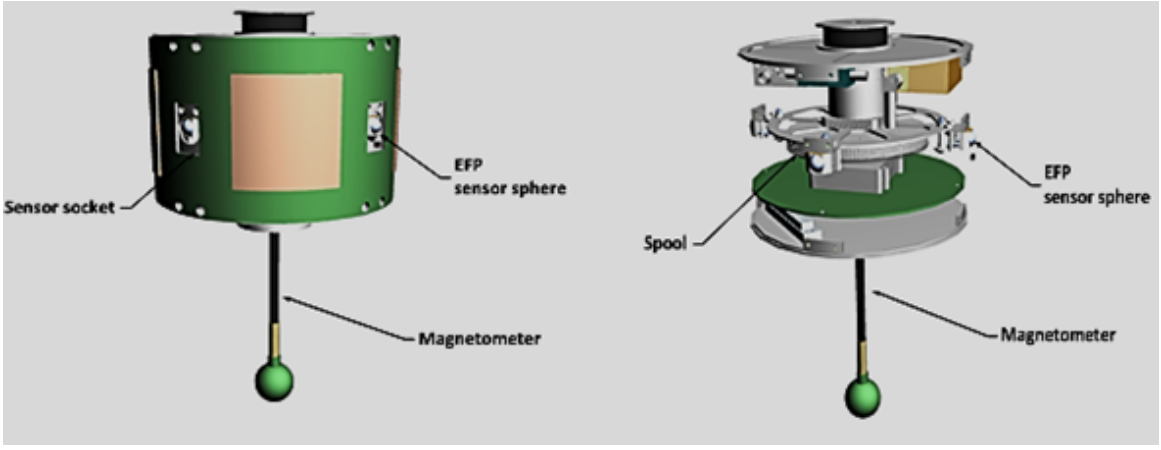

Fig. 1.5: ASSP sub-payload.

payload. Two more will then be ejected in the plus and minus down range directions, but at 25 m/s to produce a shorter baseline throughout the flight. By 400 km altitude, the start of green trajectories in Figure 1.6, the sub-payloads will have been spun up and ejected by the main payload. The miniature wire boom deployment system on ASSP payloads will deploy the electric field booms immediately after ejection from the main payload. The constellation will continue down range for another ˜700 seconds at which time the payloads will begin to pass through 120-140 km altitude range with a separation of about 50 km.

A sounding rocket flights lasts only 1000-2000 seconds [3]. Therefore, due to the short duration available for wire boom deployment as compared to orbital spacecraft like DICE, it is highly desirable to get wire boom deployment rate as high as possible within the physical limits of the system. The requirement on ASSP's wire boom deployment system is to deploy 2 meter long booms in about 20 seconds. The deployment mechanisms of DICE and ASSP are slightly different. In the DICE mission, a squiggle motor was used to limit the rotation of the spool with respect to the spinning CubeSat by applying break on the spool. The motivation behind this mechanism was to perform slow deployment. But in the latter case a piezoelectric rotary motor will be used to provide actuation for moving the wire booms out from sockets of the sub payloads (shown in Figure 1.5).

A feedback control algorithm will control the motor to deploy the wire booms. Although the deployment scheme for DICE and ASSP is dissimilar, both missions share the same concern of undesirable oscillations of the wire boom during deployment that in a worst case scenario could result in catastrophic tangling of the wire booms with each other or the spacecraft. In the case of ASSP there is a need to limit, or damp, any boom oscillations and to understand the motion of the sensors such that the analysis of the electric field data can proceed.

1.5 Thesis Overview

This thesis will examine the dynamics involved in the stable deployment of wire boom systems from CubeSats used in DICE and the sub-orbital payloads to be used in ASSP. The objective is to develop a control system for the safe deployment of the wire booms.

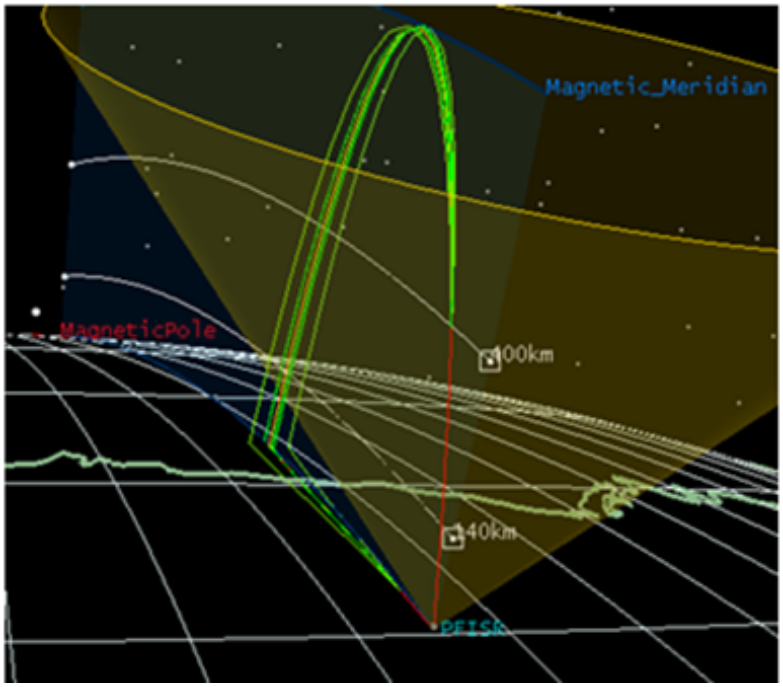

Fig. 1.6: Simulated trajectories of the ASSP main payload (red curve) and six sub-payloads (green curves) ejected along the track and across the track with apogee of 700 km and traveling 700 km down range.

The development of a control system requires the modeling of the dynamic behavior of the spacecraft and wire boom system. This model is described by a set of differential equations for the motion of the sensors and the spacecraft. The dynamics involved in the deployment of wire booms from spacecraft are based on the law of conservation of angular momentum in absence of any external torque. Several authors have described their methods and equations for the deployment of wire booms from spacecraft. Kintner and Psiaki in their paper "Rapid Energy Dissipation in a Yo-Yo-Type Wire Boom Deployment System" [3] derived a set of equations of motion for the SERRIA wire boom system on a sounding rocket. Another useful paper on the dynamics of wire boom deployment is "Dynamics of wire boom oscillations on a spinning satellite Part I, Lagrangian equations of motion and transient response" written by Lai, Mahon, and Smiddy [13]. Among important parameters to be considered for the overall system dynamics are the deflections of the tip masses from the steady state position during deployment and the spin rate of the spacecraft.

In Chapter 2, a relatively simple and limited one-dimensional model for the deployment of a wire boom system is first described. In this model, the out of plane deflections as well as the in plane deflections of the deploying wire booms and the mass of the wires are ignored. The differential equations derived are simulated using Simulink® to aid in the understanding of the deployment process and to correct and refine the dynamical model. Next a two-dimensional wire boom deployment model is developed with full nonlinear dynamics. This model is used to observe the effects of different deployment profiles on the in-plane oscillations of the wire booms. In Chapter 3, a proportional plus integral controller will be used to control the deployment profile of the wire booms. Then a more complex design methodology adopted for nonlinear systems will be presented in which the nonlinear dynamics involved in the one-dimensional model will be linearized into a state space form. A controller designed on the state space model will be tested on both the nonlinear dynamics. The simulation of the controlled deployment will also be done in Simulink®. Chapter 4 will provide the simulation results for the one-dimensional model first without making use of controller, i.e. without the operation of break force on the spool, and then for the controlled deployment. The deployment results will be presented in the form of plots obtained from the simulations done in Simulink®. A robustness check on the controller's performance will be then presented for different spin rates which may be acquired by the spacecraft before deploying the wire booms. This chapter will also present a study on slow and fast deployment scheme in terms of the in-plane oscillations obtained while simulating the two dimensional model for DICE and ASSP missions. Chapter 5 will present a concluding summary and results with an insight to promising future work in this research problem.

Chapter 2

Wire Boom Deployment System Dynamics

A spacecraft free of external torques and spinning about the largest of its principal moments of inertia (major axis spinner) is in the lowest energy state possible for its rational motion and is therefore robustly stable. Under these conditions the angular momentum of the spacecraft is constant. The DICE and ASSP mission make use of crossed wire boom systems. All four electric field sensors are deployed on wire booms simultaneously via unwinding from a common spool. An incremental extension of the wire booms increases the principal moment of inertial of the spacecraft and thus decreases the spin frequency due to conservation of angular momentum. The minimum energy state of the system also decreases with the larger inertia leaving an incremental amount of energy in the system. This is because the rotational energy depends upon the square of the angular velocity while the angular momentum depends linearly. This excess energy, or freed energy, must be dissipated from the system for the spacecraft to be in a stable spin state. Depending on the wire boom release mechanism design and its function some, or all, of the excess energy will be initially dissipated as work against this release mechanism. The remaining energy becomes the free internal energy of the system and will manifest as pendulum oscillation of the wire booms and/or coning motion of the spacecraft body. Over time, this free energy will be dissipated in the form of heat by flexing of the wire or at the attachment site of the booms to the spacecraft.

In this chapter, we develop two models for the deployment of wire booms from DICE and ASSP. The first model is developed for the length of a wire as it deploys from the spool system under the centrifugal force acting on the weighed sensor. The only opposing force is that of the break which increases the rotational friction of the spool relative to the spacecraft body. This model is one-dimensional in terms of the boom motion in that the

sensors can only move radially away from the spacecraft. The second model includes the two-dimensional motion of the sensors in the plane perpendicular to the rotation vector or in-plane oscillations of the booms along with their effects on the rotation rate of the spacecraft body but the model is parameterized by the deployment length. A profile of the deployment length verses time must be specified and then the model reproduces the pendulum dynamics between the sensors and the spacecraft body.

The first model is used in Chapter 3 to develop a control law for the brake system of the spool and the second model is used to determine the resulting pendulum behavior of the booms during deployment in Chapter 4.

2.1 One-Dimensional Wire Boom Deployment Dynamics Model

The one-dimensional model is a relatively simple set of equations for the wire boom deployment dynamics. In this modeling approach, only translational motion of the wire booms and sensor mass is considered and deflections of the wire booms at the attachment points to the spacecraft and the mass of the boom wires are ignored. The spacecraft and the wire boom system are divided into three components: the spacecraft body with its principle moment of inertia, I_b, about the e_z axis of rotation and the spool with its principle moment of inertia, I_s, and the moment of the wire boom system, as shown in Figure 2.1 which describes the coordinate system for the model.

The value of structural parameters $r,\ a,\ l,\ m_s$ in the wire boom deployment system shown in the figure above for DICE spacecraft are given in Table 2.1.

In the absence of any external torque, the total angular momentum of the spacecraft, the spool containing the wire within the spacecraft, and the sensors are given as

$$\overrightarrow{h} = \overrightarrow{h}_b + \overrightarrow{h}_s + \overrightarrow{h}_w, \tag{2.1}$$

where $\overrightarrow{h}_b$ is the angular momentum of the spacecraft body, $\overrightarrow{h}_s$ is the angular momentum of the spool, and $\overrightarrow{h}_w$ is the angular momentum of the sensors attached at the end of the wire booms.

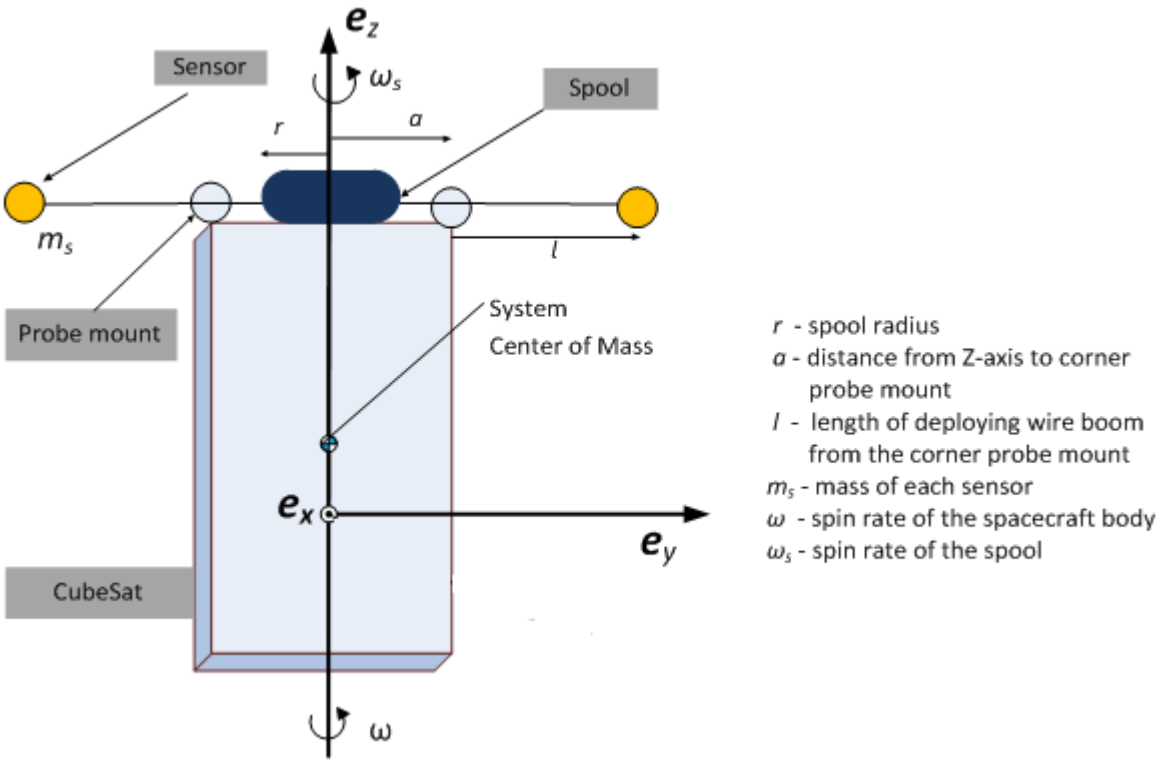

Fig. 2.1: Diagram of wire boom system during deployment consisting of the spacecraft body, the sensor mass and the spool system.

Table 2.1: Value of structural parameter for DICE wire boom deployment system.

Structural Parameter	Symbol	Value	Units
Distance from Z-axis to corner probe mount	a	5.12	cm
Wire Boom Deployment Length	l	500	cm
Spherical Sensor Mass	m_s	8.35	g
Deployment Spool Radius	r	4.75	cm
DICE CubeSat Spin rate before deployment begins	ω	2	Hz

The angular momenta can be expressed in terms of angular velocity as the product of the body's moment of inertia I and its angular velocity as

$$\vec{h}_b = I_b \vec{\omega}, \tag{2.2}$$

$$\vec{h}_s = I_s \vec{\omega}_s, \tag{2.3}$$

$$\overrightarrow{h}_w = (a+l)^2 \; m\overrightarrow{\omega}, \tag{2.4}$$

where $m\,(a+l)^2$ is the moment of inertia of the sensor deployed to a length of l and all rotation is about the e_z axis. We let $m = 4m_s$ be the total mass of all of the sensors. The rotation rate of the spacecraft body and the wire boom system is ω due to the mechanical coupling of these systems. The spool rotates independently of the body and its rotation rate in the inertial frame is called ω_s. We ignore the mass of the wire and also any deflection of the wire boom system. The angular momentum of the entire system should be conserved because there are no external forces acting on the system giving

$$\frac{dh}{dt} = 0. \tag{2.5}$$

After substituting the value of h from equation (2.1) we get

$$\frac{dh_b}{dt} + \frac{dh_s}{dt} + \frac{dh_w}{dt} = 0, \tag{2.6}$$

$$\dot{\omega} I_b + \dot{\omega_s} I_s + \omega(a+l)^2 m + 2m\omega\,(a+l)\,\dot{l} = 0, \tag{2.7}$$

where we have dropped the vector notation because the angular momentum assumed to be in the e_z direction and have used the dot notation to indicate derivatives in time. The angular displacement of the spool relative to the body is defined to be

$$\delta\omega{=}\omega_{\mathrm{s}}{-}\omega, \tag{2.8}$$

or

$$\omega_s = \delta\omega + \omega. \tag{2.9}$$

Substituting this value of ω_s in (2.7), we get

$$\dot{\omega}\left[\; I_b + I_s + m(a+l)^2 \;\right] + \omega\left[\; 2m\,(a+l)\,\dot{l} \;\right] + I_s\dot{\delta\omega} = 0. \tag{2.10}$$

The deployment length is tied to the angular displacement of the spool. Hence, the

translational displacement of the wire boom is related to angular displacement of the spool as

$$l = \delta\theta_s \; r. \tag{2.11}$$

where r is the radius of the spool. Differentiating both sides with respect to time t, we get

$$\frac{d\left(\delta\theta_s\right)}{dt} = \frac{d}{dt}\left(\frac{l}{r}\right). \tag{2.12}$$

Again differentiating both sides with respect to time, we get

$$\dot{\delta\omega} = \frac{\ddot{l}}{r}. \tag{2.13}$$

Substituting this value in equation (2.10), we get

$$\dot{\omega}\left[\; I_b + I_s + m(a+l)^2 \;\right] + \omega\left[\; 2m\,(a+l)\,\dot{l} \;\right] + \frac{I_s}{r}\ddot{l} = 0. \tag{2.14}$$

We now consider an equation to describe the extending motion of the sensors coupled with the rotation of the spool. This equation is written in the reference frame of the spacecraft and as such is non-inertial due to the spacecraft rotation. We add the centrifugal force acting on the sensor masses. This force is coupled along the wires to the spool. A breaking force is created opposite the centrifugal force by the break on the spool. It can range in value from zero to the value of the centrifugal force at any time as shown in Figure 2.2. The centrifugal force acts along the radial direction to the axis of rotation and is given as

$$F_c = m\omega^2(l+a), \tag{2.15}$$

where once again we let $m = 4m_s$ be the total mass of all of the sensors. The breaking force acts opposite the centrifugal force. The Inertial forces effecting the deployment of the sensors are due to the angular inertia of the spool, $\delta\dot{\omega}I_s$, when wire is pulled off and spins up the spool and the mass of the sensor, $m\ddot{l}$.

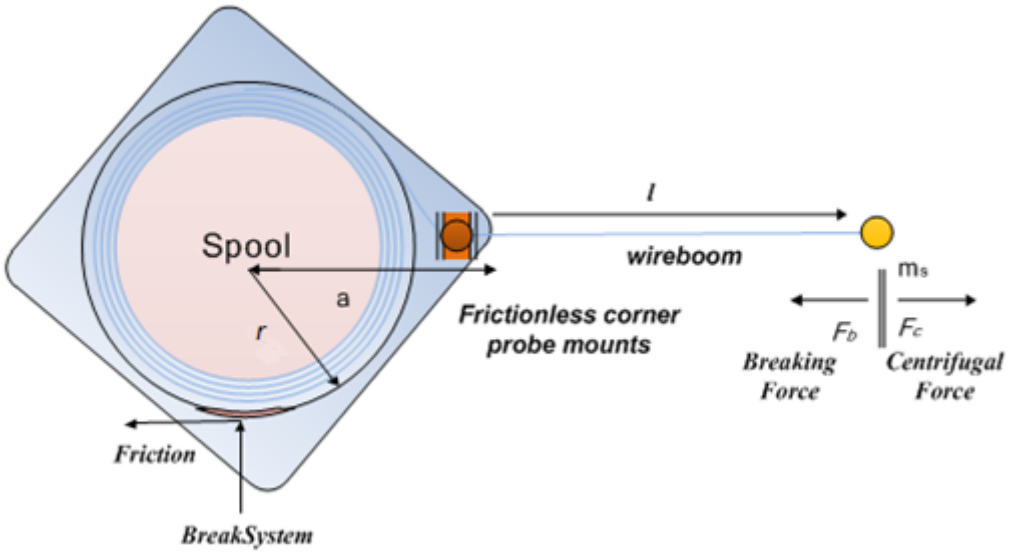

Fig. 2.2: Illustration of wire boom deployment.

The rotational motion of the spool alone is

$$(F_c - F_b)\, r = \dot{\delta\omega}\ \mathrm{I_s}; \tag{2.16}$$

and the linear motion of deploying sensors at the end of the wire boom is

$$(F_c - F_b) = m\ \ddot{l}. \tag{2.17}$$

Thus, the total force comes from combining equation (2.16) and equation (2.17), to get

$$m\ddot{l} + \dot{\delta\omega}\frac{I_s}{r} = F_c - F_b. \tag{2.18}$$

After substituting the value of centrifugal force from equation (2.15) in equation (2.18), the acceleration in the translational motion of wire booms is found to be

$$\ddot{l} = \left(\frac{mr^2}{I_s + mr^2}\right)\left[\omega^2(l+a) - \frac{F_b}{m}\right]. \tag{2.19}$$

To put this development in a standard form, we can now write the set of coupled differential equations that can solved in MATLAB®/Simulink®, as

$$\dot{\omega} = \frac{d\omega}{dt}, \tag{2.20}$$

$$\dot{\omega} = \frac{-1}{\left[I_b + I_s + m(a+l)^2\right]} \left(\omega \left[2m\left(a+l\right)\dot{l}\right] + \frac{I_s}{r}\ddot{l}\right), \tag{2.21}$$

$$\dot{l} = \frac{dl}{dt}, \tag{2.22}$$

$$\ddot{l} = \frac{d\dot{l}}{dt}, \tag{2.23}$$

$$\ddot{l} = \frac{mr^2}{mr^2 + I_s}\left(\omega^2(l+a) - \frac{F_b}{m}\right). \tag{2.24}$$

2.2 Two-Dimensional Wire Boom Deployment Dynamics Model

The derivation of the two-dimensional model is similar in many ways to the well-known double pendulum problem in physics and mathematics [14]. A double pendulum is a pendulum with another pendulum attached to its end and is a simple physical system that displays chaotic behavior with strong sensitivity to its initial conditions. We approach the model using Lagrangian mechanics and find similarities between the wire boom deployment problem and the double pendulum in the following ways. The two-point masses represent the attachment point of the wire boom to the spacecraft and the sensor at the end of the wire boom. The moment of inertia of the spacecraft about its center of mass is equivalent to the length and mass of the first pendulum. The length of the second pendulum is wire boom length and the mass is the electric field sensor mass. We modify the double pendulum problem by allowing the length of the second boom to vary with time by a specified function and ignore gravity. Because of the algebraic complexity of the problem the derivation is computed in MuPAD® which also directly produced the final code for simulation in MATLAB®.

We develop the equations for kinetic and potential energy in the inertial reference frame

described in Figure 2.3. The moment of inertia of the spacecraft at a point l_1 distance from the spacecraft's center of rotation, where the wire booms attach to the structure is modeled as $m_1 l_1^2$. The angular deflection of the spacecraft in inertial space is given by θ_1 and θ_2 give the deflection of the wire boom as illustrated in the figure. The length of the wire boom is given by l_2. The wire is assumed massless and the mass of the spherical sensor is given by m_2. Finally, we add a spring and damper system to the attachment point of the wire boom to the spacecraft. This model is intended to reproduce the in-plane defections and oscillations occurring through the process of wire boom deployment where the profile, length vs time, of the deployment is specified.

The spring and the damper act at the attachment point of the boom and the spacecraft and are modeled with a spring of constant k that acts on the deflection of the boom $(\theta_1 - \theta_2)$ and a dash pot that acts on the rate of deflection of the boom i.e. $(\dot{\theta}_1 - \dot{\theta}_2)$ with damping constant c. The dash pot slowly dissipates energy from the system over time. The size of these constants is determined by the wire properties and mechanisms at the attachment point of the wire boom to the DICE and ASSP payloads. The derivation begins by finding the Lagrangian, L from the kinetic and potential energy in the inertial coordinate system, and then deriving the differential equations of motion with respect to the generalized coordinates $\theta_1,\ \theta_2$ [14].

The positions of the masses m_1 and m_2 in Cartesian coordinates in terms of the angles θ_1 and θ_2 are given as

$$x_1 = l_1 cos\theta_1, \tag{2.25}$$

$$y_1 = l_1 sin\theta_1, \tag{2.26}$$

$$x_2 = x_1 + l_2 cos\theta_2, \tag{2.27}$$

$$y_2 = y_1 + l_2 sin\theta_2. \tag{2.28}$$

The time derivatives of the position coordinates for each of the masses are given by

$$\dot{x}_1 = -l_1 \dot{\theta_1} sin\theta_1, \tag{2.29}$$

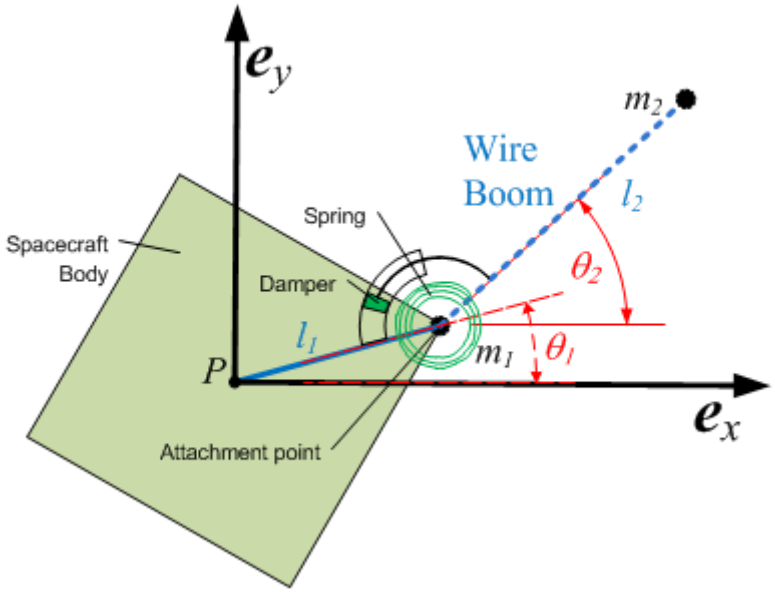

Fig. 2.3: Two-dimensional depiction of wire boom deployment.

$$\dot{y}_1 = l_1\dot{\theta}_1 cos\theta_1, \tag{2.30}$$

$$\dot{x}_2 = \dot{x}_1 + \dot{l}_2 cos\theta_2 - l_2\dot{\theta}_2 sin\theta_2, \tag{2.31}$$

$$\dot{y}_2 = \dot{y}_1 + \dot{l}_2 sin\theta_2 + l_2\dot{\theta}_2 cos\theta_2. \tag{2.32}$$

From these expressions we can calculate the kinetic energy of the spacecraft body and sensor (m_1 and m_2) under the assumption that l_1 is constant and l_2 is a function of time by

$$T = \frac{1}{2}m_1 v_1^2 + \frac{1}{2}m_2 v_2^2, \tag{2.33}$$

where

$$v_1^2 = \dot{x}_1^2 + \dot{y}_1^2, \tag{2.34}$$

$$v_2^2 = \dot{x}_2^2 + \dot{y}_2^2. \tag{2.35}$$

After substituting the values in the expression for velocity, the expression for kinetic energy for m_1 and m_2 are given as

$$T_1 = \frac{l_1^2 m_1 \dot{\theta}_1^2}{2}, \tag{2.36}$$

$$T_2 = \frac{m_2 \left(\dot{l}_2^2 + l_1^2 \dot{\theta}_1^2 + l_2^2 \dot{\theta}_2^2 - 2\dot{\theta}_1 \dot{l}_2 l_1 \sin(\theta_1 - \theta_2) \ + 2\dot{\theta}_1 \dot{\theta}_2 l_2 l_1 \cos(\theta_1 - \theta_2 \ ) \right)}{2}. \tag{2.37}$$

During the deployment of the wire booms the potential energy in the moving system will be due to the spring constant known as elastance, therefore,

$$V = \frac{1}{2} k (\theta_1 - \theta_2)^2. \tag{2.38}$$

The Lagrangian for the system can then be computed as

$$V = \frac{1}{2} k (\theta_1 - \theta_2)^2, \tag{2.39}$$

$$L = T - V, \tag{2.40}$$

$$\begin{aligned} L = \frac{m_2 \dot{l}_2^2}{2} - \frac{\theta_2^2 k}{2} - \frac{\theta_1^2 k}{2} + \theta_1 \theta_2 k + \frac{l_1^2 m_1 \dot{\theta}_1^2}{2} + \frac{l_1^2 m_2 \dot{\theta}_1^2}{2} + \frac{l_2^2 m_2 \dot{\theta}_2^2}{2} \\ - \dot{\theta}_1 \dot{l}_2 l_1 m_2 \sin(\theta_1 - \theta_2) \ + \dot{\theta}_1 \dot{\theta}_2 l_1 l_2 m_2 \cos(\theta_1 - \theta_2). \end{aligned} \tag{2.41}$$

The first Euler-Lagrange equation given as

$$\frac{d}{dt} \left(\frac{\partial L}{\partial \dot{\theta}_1} \right) - \frac{\partial L}{\partial \theta_1} + \frac{\partial D}{\partial \dot{\theta}_1} = 0, \tag{2.42}$$

$$\begin{aligned} \frac{d}{dt} \left(\frac{\partial L}{\partial \dot{\theta}_1} \right) = l_1^2 m_1 \ddot{\theta}_1 + l_1^2 m_2 \ddot{\theta}_1 - \ddot{l}_2 l_1 m_2 \sin(\theta_1 - \theta_2) \ + \ddot{\theta}_2 l_2 l_1 m_2 \cos(\theta_1 - \theta_2) \\ + \dot{\theta}_2 \dot{l}_2 l_1 m_2 \cos(\theta_1 - \theta_2) \ - \dot{l}_2 l_1 m_2 \cos(\theta_1 - \theta_2) \ \left(\dot{\theta}_1 - \dot{\theta}_2 \right) \\ - \dot{\theta}_2 l_2 l_1 m_2 \sin(\theta_1 - \theta_2) \ \left(\dot{\theta}_1 - \dot{\theta}_2 \right), \end{aligned} \tag{2.43}$$

$$\frac{\partial L}{\partial \theta_1} = \theta_2 k - \theta_1 k - \dot{\theta}_1 \dot{l}_2 l_1 m_2 \cos(\theta_1 - \theta_2) \ - \dot{\theta}_1 \dot{\theta}_2 l_2 l_1 m_2 \sin(\theta_1 - \theta_2) \ . \tag{2.44}$$

The dissipation factor due to the viscous damping from the dashpot is given as

$$D = \frac{1}{2}c\Big(\dot{\theta}_1 - \dot{\theta}_2\Big)^2. \tag{2.45}$$

Then,

$$\frac{\partial D}{\partial \dot{\theta}_1} = c\left(\dot{\theta}_1 - \dot{\theta}_2\right). \tag{2.46}$$

After substitution of the values from equation (2.46), equation (2.44), and equation (2.43) in equation (2.41), the first Euler-Lagrange equation is found as

$$\begin{aligned} &c\dot{\theta}_1 - c\dot{\theta}_2 + \theta_1 k - \theta_2 k + l_1^2 m_1 \ddot{\theta}_1 + l_1^2 m_2 \ddot{\theta}_1 - \ddot{l}_2 l_1 m_2 \sin(\theta_1 - \theta_2) \; + \ddot{\theta}_2 l_2 l_1 m_2 \cos(\theta_1 - \theta_2) \\ &+ 2\dot{\theta}_2 \dot{l}_2 l_1 m_2 \cos(\theta_1 - \theta_2) \; + \dot{\theta}_2^2 l_2 l_1 m_2 \sin(\theta_1 - \theta_2) \; = 0. \end{aligned} \tag{2.47}$$

The second Euler-Lagrange equation given by

$$\frac{d}{dt}\left(\frac{\partial L}{\partial \dot{\theta}_2}\right) - \frac{\partial L}{\partial \theta_2} + \frac{\partial D}{\partial \dot{\theta}_2} = 0, \tag{2.48}$$

$$\begin{aligned} \frac{d}{dt}\left(\frac{\partial L}{\partial \dot{\theta}_2}\right) &= \ddot{\theta}_2 l_2^2 m_2 + 2\dot{\theta}_2 l_2 \dot{l}_2 m_2 + \ddot{\theta}_1 l_2 l_1 m_2 \cos(\theta_1 - \theta_2) \\ &\quad + \dot{\theta}_1 \dot{l}_2 l_1 m_2 \cos(\theta_1 - \theta_2) \; - \dot{\theta}_1 l_2 l_1 m_2 \sin(\theta_1 - \theta_2)\left(\dot{\theta}_1 - \dot{\theta}_2\right), \end{aligned} \tag{2.49}$$

$$\frac{\partial L}{\partial \theta_2} = \theta_1 k - \theta_2 k + \dot{\theta}_1 \dot{l}_2 l_1 m_2 \cos(\theta_1 - \theta_2) \; + \dot{\theta}_1 \dot{\theta}_2 l_2 l_1 m_2 sin(\theta_1 - \theta_2), \tag{2.50}$$

$$\frac{\partial D}{\partial \dot{\theta}_2} = -c\left(\dot{\theta}_1 - \dot{\theta}_2\right). \tag{2.51}$$

After substitution of the values from equations (2.50), (2.49), and (2.48) in equation (2.47), the second Euler-Lagrange equation is found as

$$c\dot{\theta}_2 - c\dot{\theta}_1 - \theta_1 k + \theta_2 k + \ddot{\theta}_2 l_2^2 m_2 + 2\dot{\theta}_2 l_2 \dot{l}_2 m_2 + \ddot{\theta}_1 l_2 l_1 m_2 \cos(\theta_1 - \theta_2) \; - \dot{\theta}_1^2 l_2 l_1 m_2 \sin(\theta_1 - \theta_2) \; = 0. \tag{2.52}$$

The two Euler-Lagrange equations can be solved simultaneously to write separate expressions for $\ddot{\theta}_1$ *and* $\ddot{\theta}_2$ as

$$\begin{aligned}\ddot{\theta}_1 = \{&\theta_1 l_2 k - \theta_2 l_2 k + \dot{\theta}_1 l_2 c - \dot{\theta}_2 l_2 c + \dot{\theta}_1 c l_1 \cos(\theta_1 - \theta_2) \ - \dot{\theta}_2 c l_1 \cos(\theta_1 - \theta_2) \\ &+ \theta_1 k l_1 \cos(\theta_1 - \theta_2) \ - \theta_2 k l_1 \cos(\theta_1 - \theta_2) - l_2 \ddot{l}_2 l_1 m_2 \sin(\theta_1 - \theta_2) \\ &+ \dot{\theta}_2^2 l_2^2 l_1 m_2 \sin(\theta_1 - \theta_2) + \frac{\dot{\theta}_1^2 l_2 l_1^2 m_2 \sin(2\theta_1 - 2\theta_2)}{2}\} \\ &/\{l_1^2 l_2 \left(-m_2 \cos(\theta_1 - \theta_2)^{\,2} + m_1 + m_2\right)\},\end{aligned} \tag{2.53}$$

$$\begin{aligned}\ddot{\theta}_2 = \{&2 c l_1 m_1 \dot{\theta}_1 - 2 c l_1 m_1 \dot{\theta}_2 + 2 c l_1 m_2 \dot{\theta}_1 - 2 c l_1 m_2 \dot{\theta}_2 + 2\theta_1 k l_1 m_1 - 2\theta_2 k l_1 m_1 \\ &+ 2\theta_1 k l_1 m_2 - 2\theta_2 k l_1 m_2 + \dot{\theta}_2^2 l_2^2 l_1 m_2^2 \sin(2\theta_1 - 2\theta_2) \ - 2\dot{\theta}_2 l_2 \dot{l}_2 l_1 m_2^2 \\ &+ 2\theta_1 l_2 k m_2 \cos(\theta_1 - \theta_2) \ - 2\theta_2 l_2 k m_2 \cos(\theta_1 - \theta_2) \ + 2\dot{\theta}_1 l_2 c m_2 \cos(\theta_1 - \theta_2) \\ &- 2\dot{\theta}_2 l_2 c m_2 \cos(\theta_1 - \theta_2) + 2 \ \dot{\theta}_1^2 l_2 l_1^2 m_2^2 \sin(\theta_1 - \theta_2) \ - l_2 \ddot{l}_2 l_1 m_2^2 \sin(2\theta_1 - 2\theta_2) \\ &- 4\dot{\theta}_2 l_2 \dot{l}_2 l_1 m_1 m_2 + 2\dot{\theta}_1^2 l_2 l_1^2 m_1 m_2 \sin(\theta_1 - \theta_2) \ + 2\dot{\theta}_2 l_2 \dot{l}_2 l_1 m_2^2 \cos(2\theta_1 - 2\theta_2) \ \} \\ &/\{l_2^2 m_2 \left(2m_1 + m_2 - m_2 \cos(2\theta_1 - 2\theta_2) \ \right)\}.\end{aligned} \tag{2.54}$$

These two coupled nonlinear equations have been simulated within MATLAB® with a specified deployment profile $\dot{l}_2$ to study the in-plane deflections of the deploying wire boom. The simulation results will be presented in Chapter 4. This model is mostly intended towards deployment scenarios with constant wire boom deployment rates such as in DICE mission and ASSP mission. This may be further developed for generalized coordinate l_2 to achieve differential equation for $\ddot{l}_2$, i.e. acceleration in the translational motion of the wire booms.

Chapter 3

Control System Design

An incremental extension of the wire booms from their stowed position increases the principal moment of inertia of the spacecraft system and decreases the spin frequency due to conservation of angular momentum. The minimum energy state of the system also decreases with the larger inertia leaving free energy in the system. This free energy can result in pendulum motion of the wire booms within the spin plane of the spacecraft or other motions. Coupling processes through geometric misalignment of the booms with the spacecraft or through dynamic spin imbalances may result in coning of the spacecraft body and out of plane oscillations of the wire booms over time. The magnitude of all oscillations must be bound by the amount of free energy within the system. Eventually the free energy will dissipate due to energy loss mechanisms provided that the motions do not result in tangling of the booms.

3.1 Controlled Wire Boom Deployment Requirements

The primary problem to be avoided when deploying flexible wire booms in space is the tangling of the booms with each other or in getting wrapped around the spacecraft. The controlled rate of wire boom extension will ensure that there is no sudden change in the energy state of the system to avoid large pendulum motion of the wire booms and significant strain or brakeage in the wires. A controlled deployment also lessens the probability of out of plane oscillations or the spacecraft conning. Within this chapter we design a boom deployment control system for use by the DICE or the ASSP mission. Each of these missions has different requirements for the deployment of the wire booms as determined by the science and engineering teams.

Wire boom deployment requirements for DICE CubeSat:

I. The in-plane oscillations of the deploying wire booms will be less than 22 degrees.

II. The out-of-plane oscillations of the deploying wire boom will be less than 45 degrees.

III. The wire boom deployment rate will be no greater than 1 centimeter per second.

Wire boom deployment requirements for ASSP payloads:

I. The in-plane oscillations of the deploying wire booms will be less than 5 degrees.

II. The out-of-plane oscillations of the deploying wire boom will be less than 5 degrees.

III. The wire boom deployment rate will be at least 10 centimeters per second.

The main difference is that in case of on-orbit satellite the boom deployment rate was kept low so that energy dissipation will damp out any boom oscillations that may occur. Several days can be allocated for the commissioning of an EFP on a satellite before operations must commence. The ASSP program has a completely different objective in that the wire booms must be deployed quickly, within 20 seconds, so that measurements with the EFP can begin immediately given the relatively short life time of the mission.

3.2 An Introduction to Control Systems

A control system is that means by which a system or a plant can be made to behave in a desired manner. Control system can be open loop or closed loop. Open-loop control systems are those in which a desired output is given as a command to a system/plant and then the system responds to that command to give an output response. Closed-loop control systems are those which in addition to command input, plant, and its output have a feedback mechanism so that the actual response of the plant can be observed to compensate for the error which is a difference between the desired response (the input) and actual response (the output).

A controller or compensator is a component of control system which manipulates the error and changes the input command so that the actual response of the plan get close to the original desired response. These operations involved in a feedback control system can be represented by a conceptual diagram given in Figure 3.1.

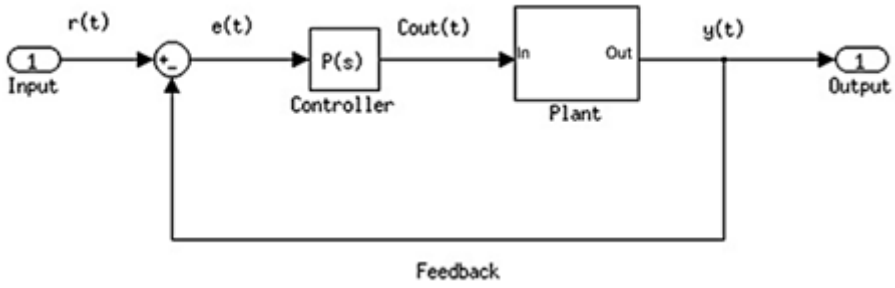

Fig. 3.1: Schematic diagram of feedback control system.

Here $r(t)$is the desired signal input, $C_{out}(t)$ is control signal fed into the plant to get output $y(t)$, and $e(t)$ is the error signal fed into the controller.

$$e(t) = r(t) - y(t) \tag{3.1}$$

The control system design can be broadly seen as a two-step process. The first step is to derive a mathematical model of system/plant dynamics for which control system is to be designed. The next step is to design a compensator for the plant. Modern control often deals with multiple-input multiple-output (MIMO) systems directly with the ordinary differential equations in the time domain. In contrast to the frequency domain analysis of the classical control theory, modern control theory utilizes the time-domain state space representation, a mathematical model of a physical system as a set of input, output, and state variables related by differential equations. Classical control approach typically deals with single-input single-output (SISO) systems using frequency domain tools which involve taking Laplace transform of the differential equations of motion and designing the controller for required performance specifications.

The use of both kinds of approaches to control the boom deployment rate is shown in this report. First a proportional plus integral (PI) controller is tested on the nonlinear deployment dynamics. The PI controller places a pole at origin and a zero at left half of the s-plane to change overall dynamics of the system [15]. PI controller falls under the classical control approach. The modern control approach shown in section 3.4 will first transform the nonlinear system into a state space format and then a controller is designed in section

3.5 to control the state variables found in the system.

3.3 Proportional Plus Integral Controller for Wire Boom Deployment Assembly of DICE Spacecraft

The control system model given below (Figure 3.2) is designed to maintain the wire boom deployment rate of 1 centimeter per second. The compensator used in this process is a proportional plus integral controller. The advantage of using a PI controller is that it makes the system immune to noise and ensures minimal steady state error and high accuracy [16].

It's a basic model used as a guideline for more complex methodology involving state space control design. The response of this system will be used to study the trajectory needed to linearize the nonlinear system dynamics. The desired deployment rate is about 1 centimeter per second. The control system to achieve the desired deployment rate of one centimeter per second (or .01 m/sec) is shown in Figure 3.2. The performance of this control system is shown in the Figure 3.3.

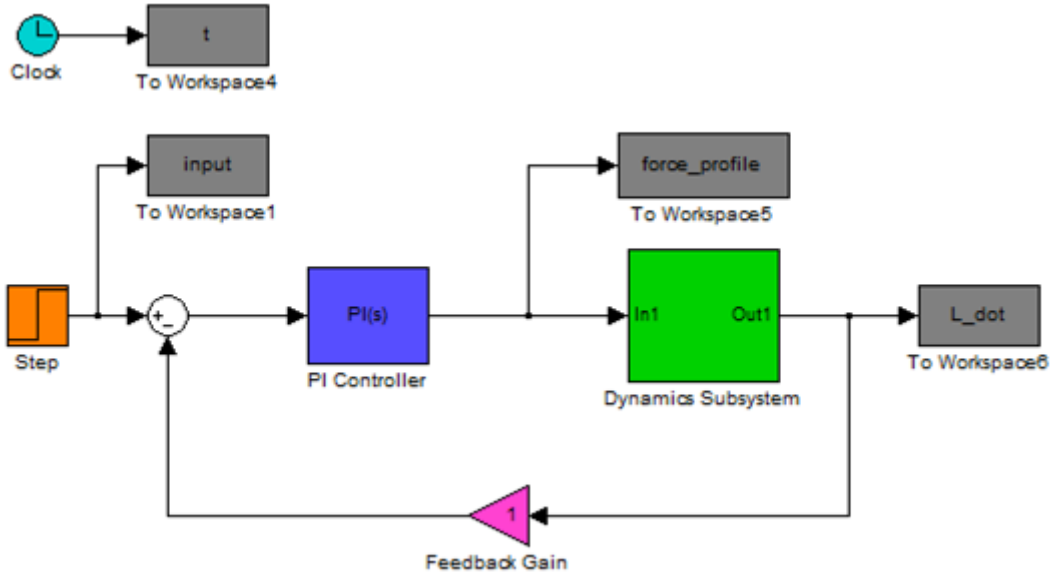

Fig. 3.2: Control system block simulated in Simulink®.

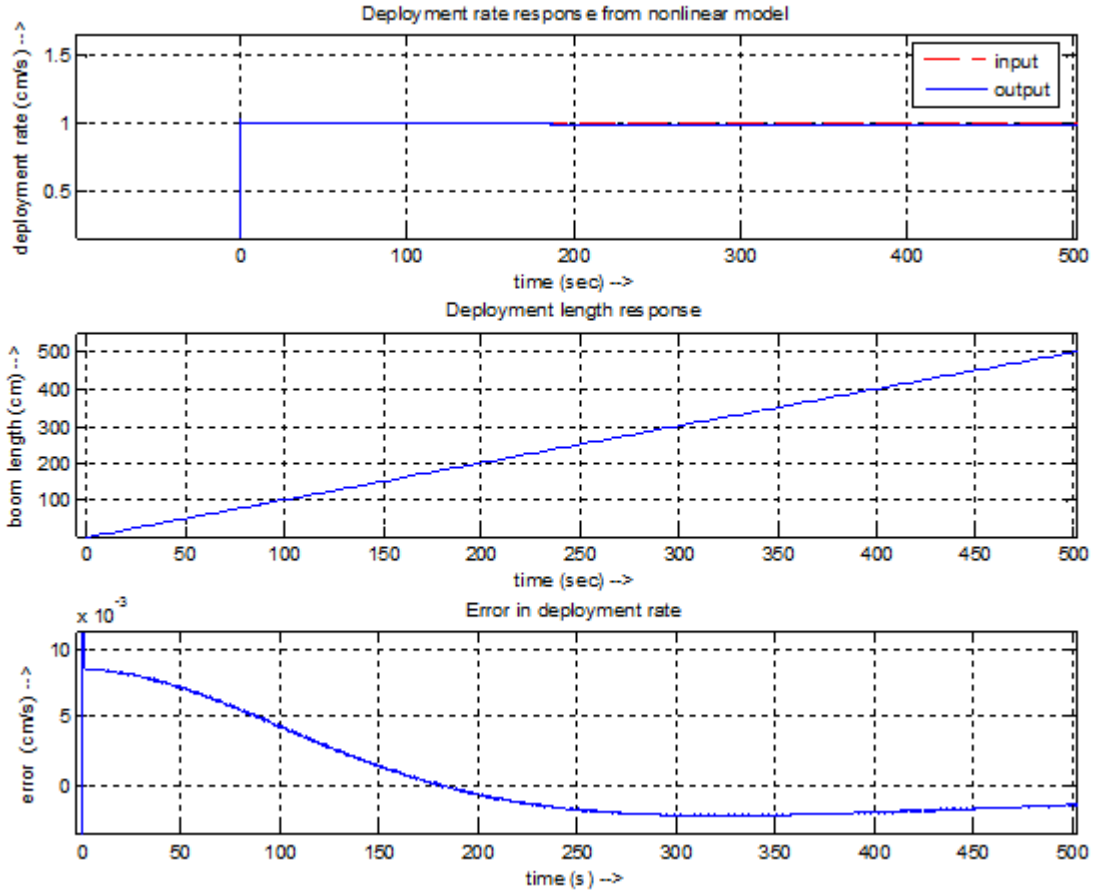

Fig. 3.3: Simulated control system output.

The proportinal plus intergral controller produces a signal $C_{out}(t)$ proportional to the error and its integral over time. It is used to minimize the steady state error over time.

$$C_{out}(t) = K_P \ .e + K_I \int_o^t e(\tau).d\tau \tag{3.2}$$

The signal generated from the controller gives required brake force input to the plant dynamics to produce the desired response. The values of K_p and K_I are -9 and -90. These gains were tuned using SIMULINK® PI controller block. Initially, a proportional controller was used to give a stable response which was then improved by adding the integrator. These gain values were found by hit-and-trial method with the SIMULINK® model.

The performance of this control system is meets the requirement of controlled deployment rate of 1 centimeter per second. It can observed from the deployment rate error plot that the error in the deployment rate is less than 1% of desired deployment rate of 1 centimeter per second. The detailed simulation results are presented in the next chapter will show that the peak value of required brake force for this controlled deployment is 0.815 N which is well below the structural limit of 1.8 N for DICE CubeSat.

3.4 State Space System Modeling and Linearization

The differential equations of motion for the one-dimensional model were derived in Chapter 2. These were

$$\dot{\omega}\left[\ I_b + I_s + m(a+l)^2\ \right] + \omega\left[\ 2m\,(a+l)\,\dot{l}\ \right] + \frac{I_s}{r}\ddot{l} = 0, \tag{3.3}$$

$$\ddot{l} = \left(\frac{mr^2}{I_s + mr^2}\right)\left[\omega^2(l+a) - \frac{F_b}{m}\right]. \tag{3.4}$$

The system given by equations (3.3) and (3.4) is a nonlinear system. In modern control system design the dynamic system is represented in a state space model. The state space model linearizes the nonlinear differential equations on given operational points of the system's dynamics. There are three states in the system: the deployment rate of the wire booms, the deployed length of the wire booms, and the CubeSat's spin frequency, given as $\dot{l}$, l, and ω. The expressions for the time derivative of each state required for the state space model are found next.

From equation (3.4) it is clear that the acceleration in the translational motion of wire booms is a function of CubeSat's spin frequency, the deployed length, and the braking force on the rotating spool by the brake control system. Therefore, it can be written as

$$\ddot{l} = f_1\left(\omega, l, F_b\right). \tag{3.5}$$

After substituting the value of $\ddot{l}$ from equation (3.4) into equation (3.3) the expression for the deployment rate is found to be

$$\dot{l} = -\frac{\dot{\omega}\left[\ I_b + I_s + m(a+l)^2\ \right]}{[2\omega m\,(a+l)]} - \frac{\frac{I_s}{r}\left(\frac{mr^2}{I_s+mr^2}\right)\left[\omega^2\,(l+a) - \frac{F_b}{m}\right]}{[2\omega m\,(a+l)]}, \tag{3.6}$$

or

$$\dot{l}\ = f_2(\dot{\omega},\ \omega,\ l,\ F_b). \tag{3.7}$$

Similarly, the expression for the spacecraft spin frequency is found to be

$$\dot{\omega} = -\frac{\omega\left[\ 2m\,(a+l)\,\dot{l}\ \right]}{\left[\ I_b + I_s + m(a+l)^2\ \right]} - \frac{\frac{I_s}{r}\left(\frac{mr^2}{I_s+mr^2}\right)\left[\omega^2\,(l+a) - \frac{F_b}{m}\right]}{\left[\ I_b + I_s + m(a+l)^2\ \right]}, \tag{3.8}$$

or

$$\dot{\omega} = f_3(\dot{l},\ \omega,\ l,\ F_b). \tag{3.9}$$

The standard state space form is given as

$$\dot{x}(t) = Ax(t) + Bu(t), \tag{3.10}$$

$$y = Cx(t). \tag{3.11}$$

Equation (3.10) is the set of differential equations involved in the dynamics. Matrix A is known as "state matrix." Matrix B is the "input matrix," and Matrix C is the "output matrix." For a system having n state variables $\{x_1(t),\ x_2(t),\ x_3(t), \ldots, x_n(t)\}$, p inputs and q outputs, the dimensions of matrix $A,\ B,\ and\ C$ will be n X $n,\ n\ X\ p,$ and $q\ X\ n$.

The system under consideration has three states. Thus the state space model will be of the form

$$\begin{bmatrix} \ddot{l} \\ \dot{l} \\ \dot{\omega} \end{bmatrix} = \begin{bmatrix} A_{11} & A_{12} & A_{13} \\ A_{21} & A_{22} & A_{23} \\ A_{31} & A_{32} & A_{33} \end{bmatrix} \begin{bmatrix} \dot{l} \\ l \\ \omega \end{bmatrix} + \begin{bmatrix} B_1 \\ B_2 \\ B_3 \end{bmatrix} F_b. \tag{3.12}$$

The Matrix A is Jacobian of three functions $f_1,\ f_2$, and f_3 with respect to the state variables $\dot{l},\ l$, and ω. It is given as

$$A = \begin{bmatrix} \frac{\partial f_1}{\partial \dot{l}} & \frac{\partial f_1}{\partial l} & \frac{\partial f_1}{\partial \omega} \\ \frac{\partial f_2}{\partial \dot{l}} & \frac{\partial f_2}{\partial l} & \frac{\partial f_2}{\partial \omega} \\ \frac{\partial f_3}{\partial \dot{l}} & \frac{\partial f_3}{\partial l} & \frac{\partial f_3}{\partial \omega} \end{bmatrix}. \tag{3.13}$$

The input Matrix B is given as

$$B = \begin{bmatrix} \frac{\partial f_1}{\partial F_b} \\ \frac{\partial f_2}{\partial F_b} \\ \frac{\partial f_3}{\partial F_b} \end{bmatrix}. \tag{3.14}$$

The elements of the state matrix and the input matrix found by performing the partial differentiations given in equation (3.13) and (3.14) are as follows:

$$\frac{\partial f_1}{\partial \dot{l}} = 0, \tag{3.15}$$

$$\frac{\partial f_1}{\partial l} = \frac{mr^2w^2}{I_s + mr^2}, \tag{3.16}$$

$$\frac{\partial f_1}{\partial \omega} = \frac{2mr^2w\,(a+l)}{I_s + mr^2}, \tag{3.17}$$

$$\frac{\partial f_2}{\partial \dot{l}} = 1, \tag{3.18}$$

$$\frac{\partial f_2}{\partial l} = \frac{\dot{\omega}\left(I_b + I_s + m(a+l)^2\right) + \frac{I_s mr\left(\omega^2(a+l) - \frac{F_b}{m}\right)}{I_s + mr^2}}{2\omega m(a+l)^2} - \frac{2\dot{\omega}m\,(a+l) + \frac{I_s mr\omega^2}{I_s + mr^2}}{2\omega m\,(a+l)}, \tag{3.19}$$

$$\frac{\partial f_2}{\partial \omega} = \frac{\omega\left(I_b + I_s + m(a+l)^2\right) + \frac{I_s mr\left(\omega^2(a+l) - \frac{F_b}{m}\right)}{I_s + mr^2}}{2\omega m(a+l)^2} - \frac{I_s r}{I_s + mr^2}, \tag{3.20}$$

$$\frac{\partial f_3}{\partial \dot{l}} = -\frac{2\omega m\,(a+l)}{I_b + I_s + m(a+l)^2}, \tag{3.21}$$

$$\frac{\partial f_3}{\partial l} = \frac{2m\left(a+l\right)\left(2\omega m\left(a+l\right)\dot{l} + \frac{I_s mr\left(\omega^2(a+l) - \frac{F_b}{m}\right)}{I_s+mr^2}\right)}{\left(I_b + I_s + m(a+l)^2\right)^2} - \frac{\left(2\omega m\dot{l} + \frac{I_s mr\omega^2}{I_s+mr^2}\right)}{\left(I_b + I_s + m(a+l)^2\right)}, \tag{3.22}$$

$$\frac{\partial f_3}{\partial \omega} = -\frac{2m\dot{l}\left(a+l\right) + \frac{2I_s mr\omega(a+l)}{I_s+mr^2}}{I_b + I_s + m(a+l)^2}, \tag{3.23}$$

$$\frac{\partial f_1}{\partial F_b} = -\frac{r^2}{I_s + mr^2}, \tag{3.24}$$

$$\frac{\partial f_2}{\partial F_b} = \frac{I_s r}{2\omega m\left(a+l\right)\left(I_s+mr^2\right)}, \tag{3.25}$$

$$\frac{\partial f_3}{\partial F_b} = \frac{I_s r}{\left(I_s+mr^2\right)\left(I_b + I_s + m(a+l)^2\right)}. \tag{3.26}$$

The linear model achieved from equation (3.15) to (3.26) is then used to find controller gains and observe controller's response on the nonlinear model.

3.5 Controller Design

In order to control to the response of the wire boom deployment system, an LQR controller is used. Linear quadratic regulator involves a mathematical algorithm that minimizes a cost function with weighting factors supplied into that algorithm. The cost function can be seen as a sum of the deviations of key measurements from their desired values. So, this algorithm finds those controller settings that minimize the undesired deviations. The LQR algorithm calculates the optimal gain Matrix K.

For a continuous time system, the state-feedback law given by equation (3.25) minimizes the quadratic cost function given by equation (3.28).

$$u = -Kx \tag{3.27}$$

$$J\left(u\right) = \int_0^\infty \left(x^T Q x + u^T R u\right) dt \tag{3.28}$$

The cost function is subject to the system dynamics

$$\dot{x} = Ax + Bu. \tag{3.29}$$

In order to find the state-feedback gain K,LQR algorithm returns the solution S of the associated Riccati equation

$$A^T S + SA - SBR^{-1}B^T S + Q = 0. \tag{3.30}$$

K is derived from S using

$$K = R^{-1}B^T S. \tag{3.31}$$

The closed-loop eigenvalues are given as

$$e = eig(A - B * K). \tag{3.32}$$

The advantage of LQR controller is that the LQR algorithm is an automated way of finding an optimal state-feedback controller. The LQR controller has been extensively used in the field of aerospace [17]. The limitation of LQR algorithm is that one needs to specify the weighting factors Q and R and compare the results with the specified design goals. It means that controller synthesis will be an iterative process where one has to find among different values of Q and R to find a set most suitable to the desired system behavior.

To find the LQR controller gain, the nonlinear system is first linearized on the operating point

$$\dot{l} = .002\ m/s, \tag{3.33}$$

$$l = .005\ m, \tag{3.34}$$

$$\omega = 12.5664\ rad/s \quad or \quad 2 \quad Hz. \tag{3.35}$$

The operating points for linearization are chosen from the set of possible initial conditions which resulted better control authority over the nonlinear dynamics. The resulting

state space system matrices are as follows:

$$A = \begin{bmatrix} 0 & 157.9137 & 1.4125 \\ 1.0000 & 0 & 0 \\ -0.1314 & -0.0047 & -0.0000 \end{bmatrix}, \tag{3.36}$$

$$B = \begin{bmatrix} -206.2706 \\ 0 \\ 0 \end{bmatrix}, \tag{3.37}$$

$$C = \begin{bmatrix} 1 & 0 & 0 \\ 0 & 1 & 0 \\ 0 & 0 & 1 \end{bmatrix}. \tag{3.38}$$

Among several tried combinations for the weights Q and R which have to be fed in LQR algorithm, the following were found to be most suitable with regards to the controller performance

$$Q = \begin{bmatrix} 4 & 0 & 0 \\ 0 & 2 & 0 \\ 0 & 0 & 1 \end{bmatrix}. \tag{3.39}$$

$$R = 4 \tag{3.40}$$

The LQR gain calculated in MATLAB® is found to be

$$K = [\ -1.0087 \quad -1.7462 \quad 0.4888\ ]. \tag{3.41}$$

The LQR controlled system is simulated in Simulink®. The block diagram of the model is shown in Figure 3.4.

The inputs to this control system are the desired state profiles namely deployment rate, deployment length, and CubeSat's angular frequency. The deployment rate is a step input which sets at the value of 1 centimeter per second after .25 of a second. With constant

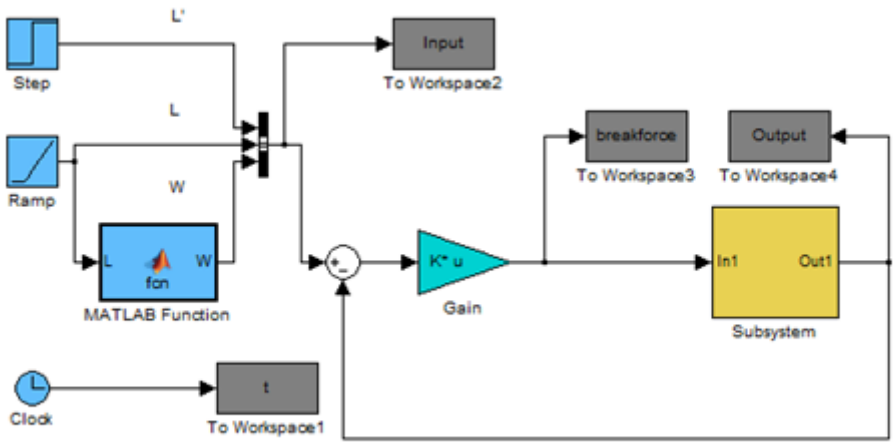

Fig. 3.4: Control system block for linear and nonlinear dynamics simulated in Simulink®.

deployment rate the deploying length is linearly dependent on the simulation time; therefore, it is given by linearly increasing ramp function with slope of 1 cm/s. It was found from the PI controller model that after deploying 5 meters of wire boom the angular velocity of the CubeSat reduced to 3.7 rad/s. Therefore, the third input which is angular frequency of the CubeSat is dependent on the length of the extending wire booms. The value of this input is dependent of the deployed length of the wire boom. The relationship is given as

$$\omega = \frac{H}{I_{sc} + 4m_s l^2}, \tag{3.42}$$

where I_{sc} is moment of inertia of the CubeSat about z axis.

The control systems performance on the nonlinear dynamics is given in Figure 3.5. The given inputs (in black) to the control system are the desired state values of deployment rate, deployment length, and CubeSat's spin rate. It can be observed that the controller is able is follow the desired trajectory of deployment (response shown in blue). The deployment of 5 meter boom length takes place slightly before than 500 seconds. Detailed simulation results along with the error in the states are presented in the next chapter.

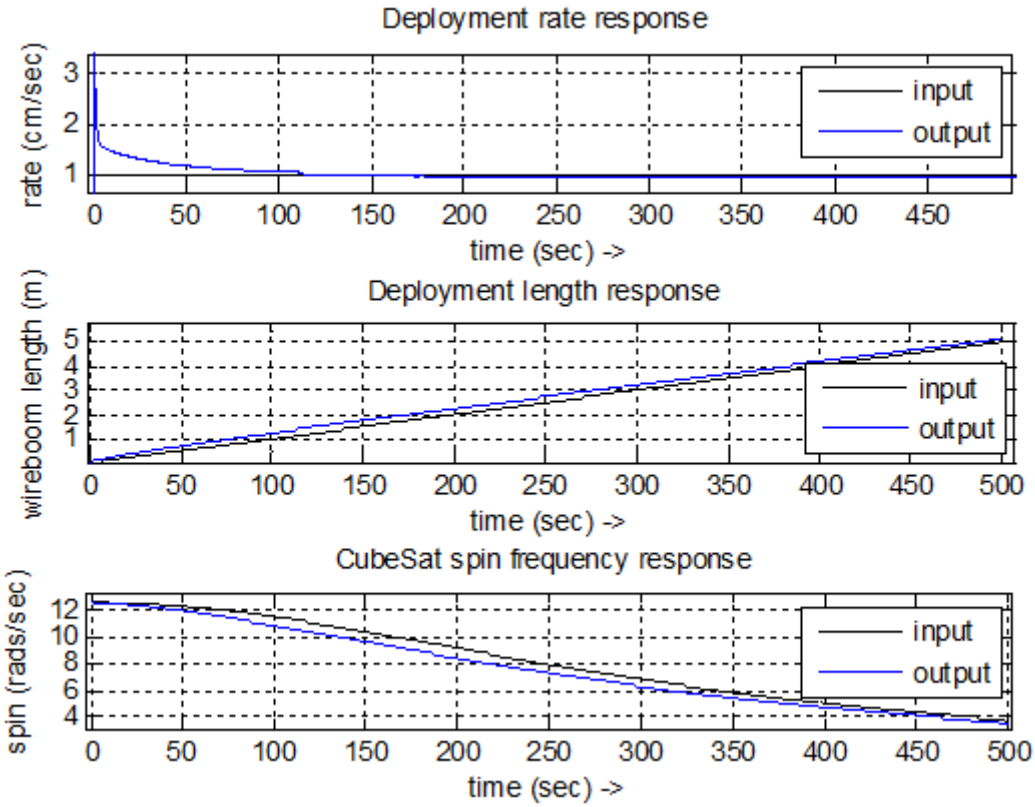

Fig. 3.5: Wire boom deployment performance of LQR controller on nonlinear dynamics.

Chapter 4

Simulation Results

4.1 Wire Boom Deployment Simulation for One-Dimensional Model

The one-dimensional wire boom deployment model was presented earlier in section 2.1. In this section, the simulation results of this model presented. This simulation is done for free deployment of the wire boom from spinning CubeSat, i.e. without any application of brakes on spool. The mechanical parameters of the wire boom deployment system used in this simulation for DICE CubeSat are given in Table 4.1. The diagram of this system was given by Figure 2.5.

The moment of inertia of spool about z-axis will be of the order of 10^{-5} Kg-m^2, therefore, the simulation is done for a simple case of $I_s = 0$ And $F_b = 0$.

I_s is the moment of inertia of the spool and F_b is the brake force to be applied on the spool to control the rate of deployment. The equations (2.21) and (2.24) can be further simplified to get

$$\dot{\omega}[I_b + m(a+l)^2] = -\omega[2m(a+l)\dot{l}], \tag{4.1}$$

$$\ddot{l} = \omega^2(l+a). \tag{4.2}$$

Table 4.1: DICE spacecraft and wire boom parameters.

Mechanical Property	Symbol	Value	Units
Moment of Inertia of Spacecraft along z-axis(Scissor and Antenna Deployed)	I_b	5.21E-02	Kg-m^2
Attachment offset	a	5.12	cm
Wire Boom Deployment Length	l	500	cm
Spherical Sensor Mass	m_s	8.35	g
Sensor Radius	r_s	0.498	cm
Deployment Spool Mass	m_{sp}	75	g
Deployment Spool Radius	r	4.75	cm
Spin Rate Before Deployment	ω	2	Hz

The Simulink model used to simulate the dynamics for one-dimensional dynamics is shown in Figure 4.1. In the Simulink® model shown in Figure 4.1, the three embedded functions calculate the value of the following expressions.

Translational acceleration:

$$L_{dd}(or\ \ddot{l}\ ) = \frac{mr^2}{mr^2 + I_s}(\omega^2(l+a) - \frac{F_b}{m});$$

rotational acceleration:

$$\omega_d\ (or\ \dot{\omega}\ ) = \frac{-1}{[I_b + I_s + m(a+l)^2]}(\omega[2m(a+l)\dot{l}] + \frac{I_s}{r}\ddot{l});$$

and angular momentum:

$$H = I_b\omega_b + I_s\omega_s + (a+l)^2 m\omega_b.$$

These values were derived in Chapter 2.

Figure 4.2 provides the plot of wire boom deployment rate with deployment time as well as the deployed wire boom length. It can be observed that it takes about .45 seconds to deploy 5 meters of wire booms from the Dice CubeSat spinning at 2 hertz about its principle axis. The exponential rise in the rate of deployment as well as the deployed length shows that the open-loop system is unstable. One of the interesting facts of the feedback control system is that it can stabilize the given unstable system to perform in a desired way. Section 4.3 of this chapter will provide the simulation results of this system controlled with a feedback PI controller.

As wire booms extend from the spool of the CubeSat, the spin frequency decreases to comply with the law of conservation of angular momentum in absence of external torque. The decrease in the CubeSat's angular frequency is shown in Figure 4.3. The centrifugal force acting on the spherical sensors of the boom, depends on the frequency of the spinning CubeSat, given by equation (2.9), and so it is expected to decrease with the decreasing spin frequency. Figure 4.4 shows decreasing centrifugal force on the sensor spheres.

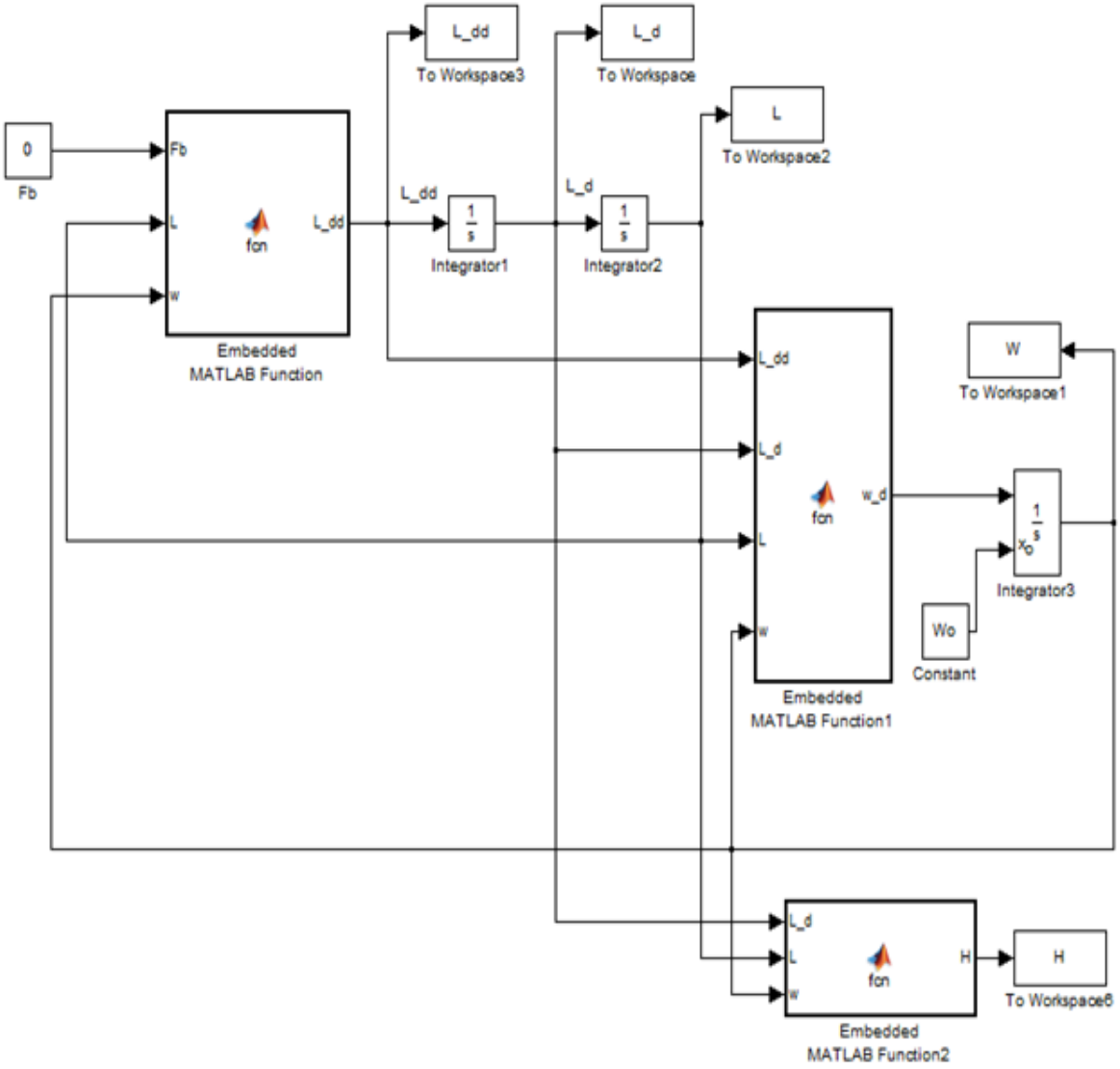

Fig. 4.1: Simulink model for one-dimensional wire boom deployment dynamics.

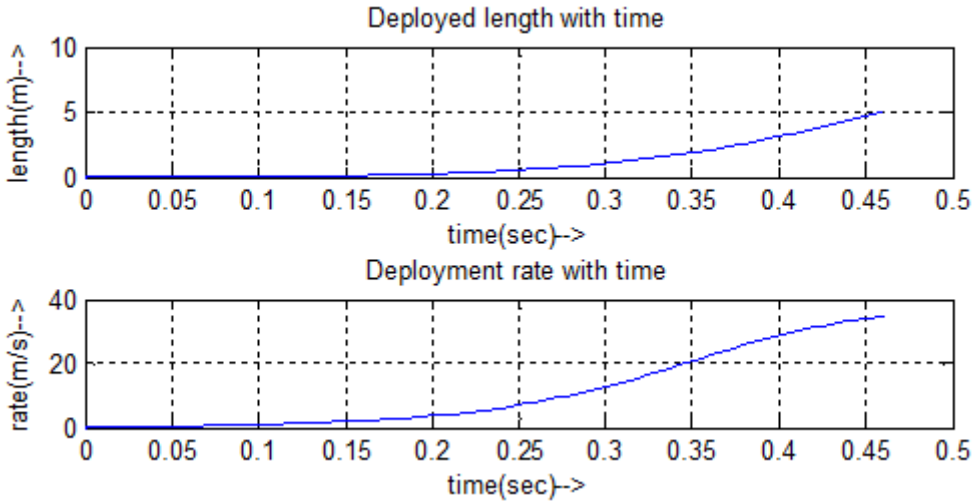

Fig. 4.2: Plot of deployed length and deployment rate with time.

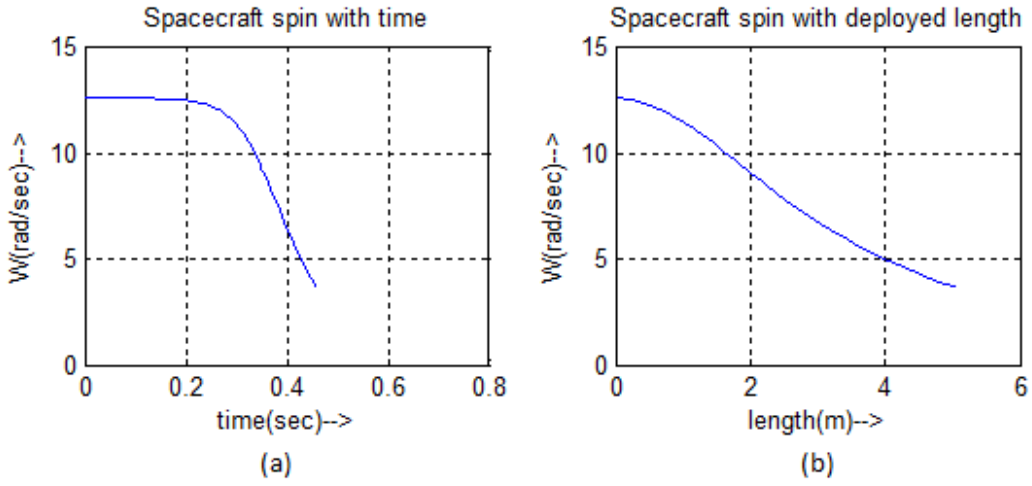

Fig. 4.3: Plot of DICE CubeSat's spin profile with (a) time, and (b) deployed wire boom length.

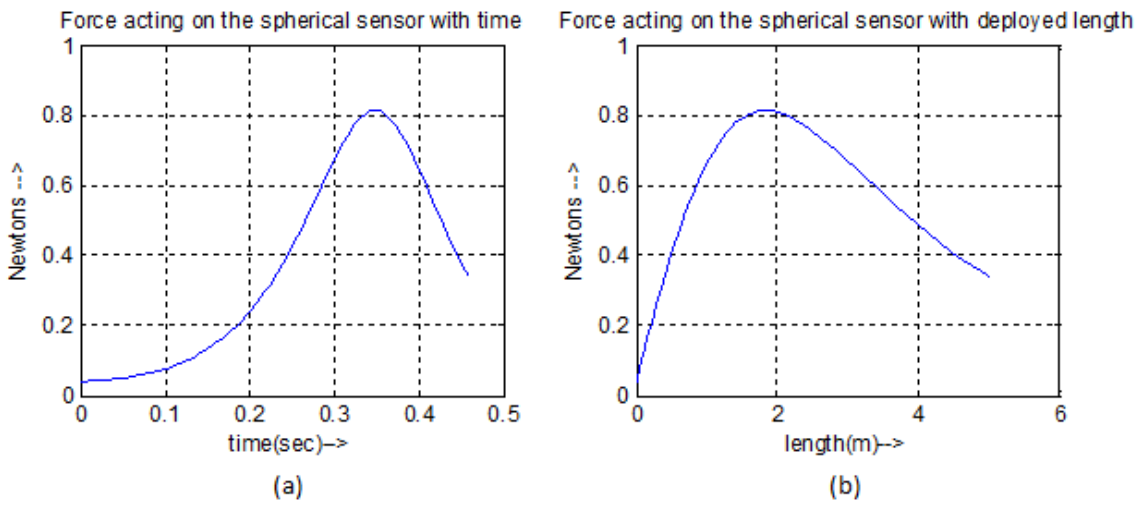

Fig. 4.4: Plot of centrifugal force on spherical sensors with (a) deployment time, and (b) deployed wire boom length.

4.2 PI Controller Results

In this section, the simulation results of the PI control system given in section 3.4 are provided. The schematic of the control system was shown in the Figure 3.2. The simulation results from this controller model give an insight into the operating points of the three states: deployment length, deployment rate, and CubeSat's spin frequency required for linear controller model.

Figure 4.5 gives the plot of the deployed wire boom length as well as the rate of deployment with time. The plot shows that the deployment of 5 meters of wire boom length was done in desired time of 500 seconds. It also shows that the controlled deployment rate settles at the desired value of 10e-3 m/s or 1 cm/s.

Figure 4.6 provides an enhanced view of the deployment rate with respect to the deployment time as well as deployment length. It shows that the controller performance is quite satisfactory as it is able to control the rate with less than 1.5% steady state error. Figure 4.7 gives the decreasing curve of the CubeSat's spin frequency with extension in wire boom length. The spin frequency is found to be decreasing from initial value of 12.5664 radians per second to about 3.7 radians per second. Figure 4.8 provides the plot of angular

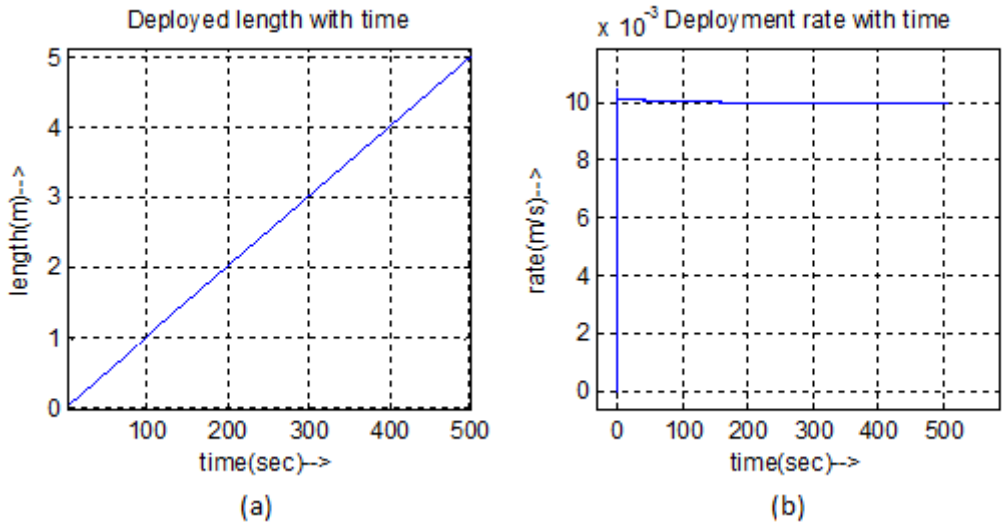

Fig. 4.5: Plot of (a) deployed wire boom length with time, and (b) wire boom deployment rate with time.

momentum of the spinning CubeSat system during the wire boom deployment. The angular momentum of a system should remain unchaged if there is no external torque on the system. According to the deployment scheme, the attitude control system of the CubeSat spins it to 2 Hz and then shuts down, therefore during the deployment there is no external torque acting on the system. Figure 4.9 shows the required brake force generated by the squiggle motor actuated brake system acting on the CubeSat's spool to control the deployment of the wire booms.

4.3 LQR Controller Results

In this section, the simulation results of a linear quadratic regulator (LQR)-based control system, given in section 3.6, are provided. The schematic of the control system was shown in the Figure 3.4. This controller is designed on the state space model with linearized dynamics and tested on the nonlinear model. The steps involved in finding the controller gain are given in section 3.6 of the previous chapter. The responses from the nonlinear model are more important compared to the linear model since the linear model is only used to find controller gain for the nonlinear dynamics. Figure 4.10 gives the deployed length

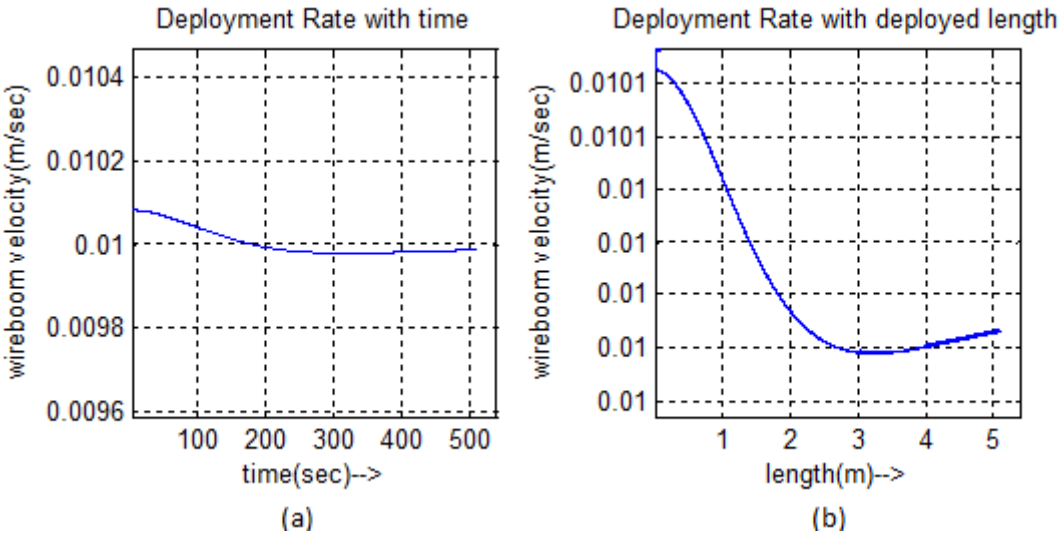

Fig. 4.6: Plot of wire boom deployment rate (a) with time, and (b) with deployed length.

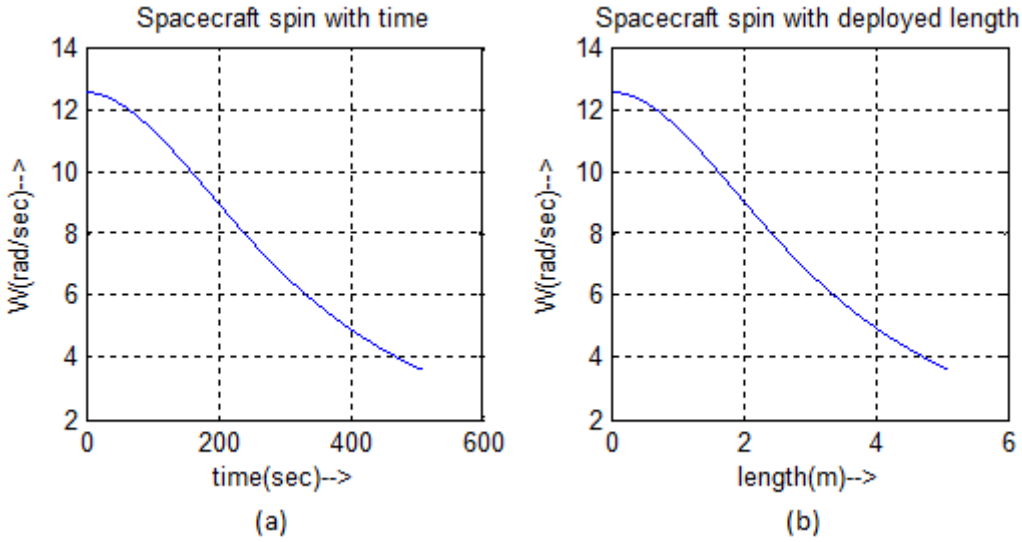

Fig. 4.7: Plot of the CubeSat's spin (a) with time, and (b) with deployed length.

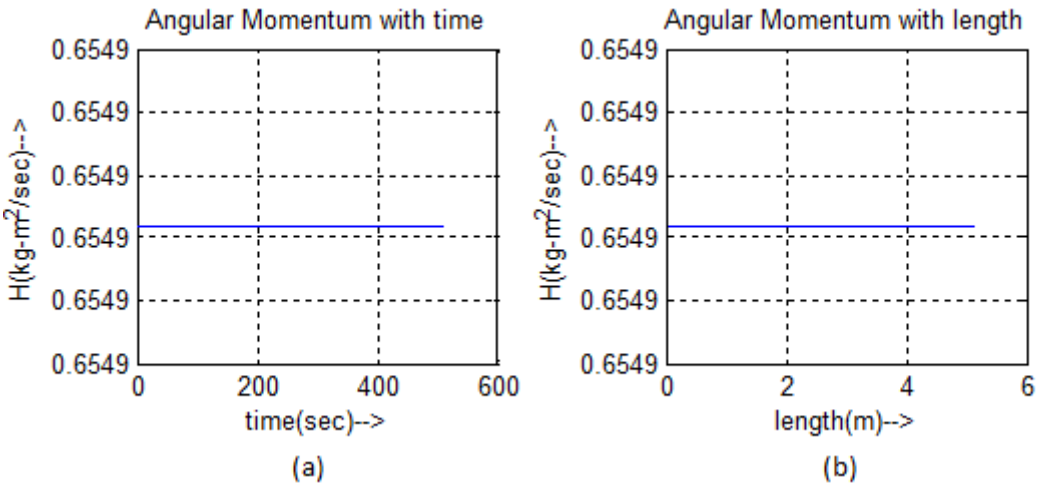

Fig. 4.8: Plot of system's angular momentum (a) with time, and (b) with deployed length.

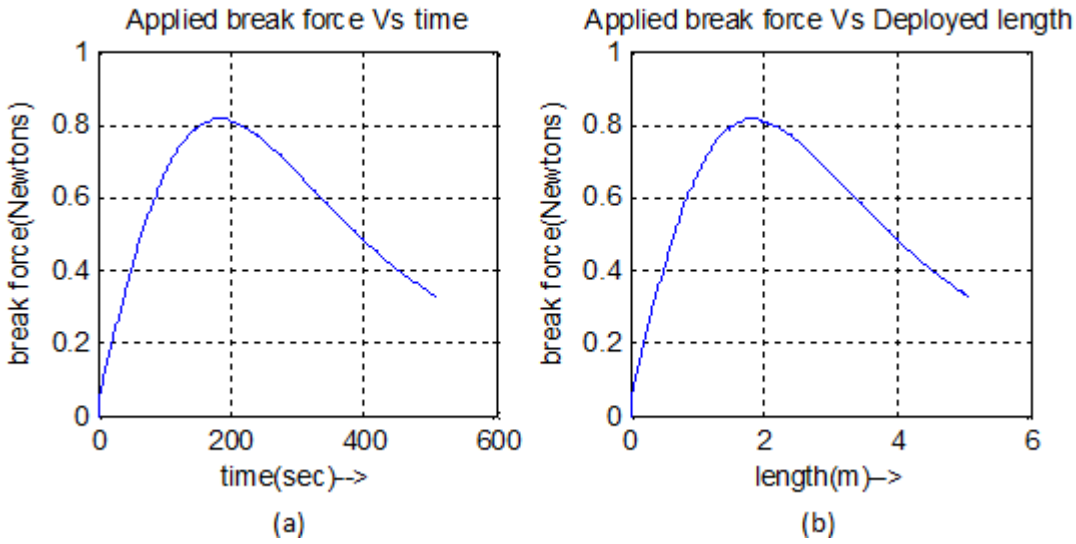

Fig. 4.9: Plot of brake force on the spool (a) with time, and (b) with deployed length.

of the wire booms as output and the difference in input and output as error of the LQR controller on the nonlinear model.

The black colored curve shows the performance desired from the control system which is fed as an input into the control system. The blue colored curve is the response (or output) of the control system. The LQR-based control system is deploying 5 meters of wire boom in 485 seconds.

Figure 4.11 gives the deployment rate control response of the LQR controller on the linear and nonlinear model. The input (shown in black color) is the desired wire boom deployment rate set as 1 cm/s. After initial overshoot to about 4.5 cm/s the controller keeps the steady state value of deployment rate close to 0.95 cm/s.

Figure 4.12 shows the response of the controller on the third state, i.e. CubeSat's spin frequency in the wire boom deployment system dynamics. It was seen from the Pi controller results that while deploying 5 meters of wire boom length the spin frequency of the CubeSat decreased from 12.5664 radians per second to about 3.7 radians per second. This spin frequency profile used as third input is shown in black.

Figure 4.13 shows the required brake force to be applied on the CubeSat's spool by the squiggle motor based brake system. The plot of the required brake force for nonlinear model with PI (shown in Figure 4.9) as well as LQR controller is quite similar.

4.4 Controller Robustness Check

In this section, a robustness check is done on PI and the LQR controllers for cases when the CubeSat would be spun up to 3 Hz and 4 Hz before deploying the wire booms. Table 4.2 provides a comparison of the simulation results for 2, 3, and 4 Hz spin frequencies below.

It is clear from the table that the performance of the PI control system starts degrading with rise in the value of the CubeSat's spin frequency. One of the factors, which puts higher limit on the value to which spin frequency of the CubeSat can be set before deploying the wire booms, is the amount of brake force which can be applied by the brake assembly on the rotating spool of the CubeSat. From the simulations it has been found that the peak

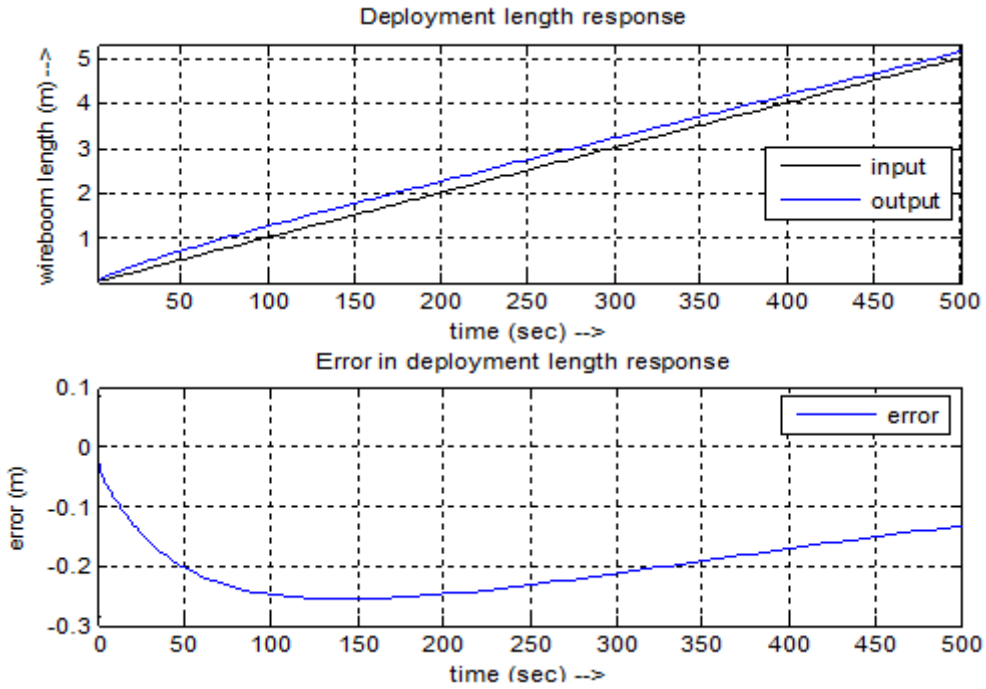

Fig. 4.10: Plot of deployed wire boom length and the resulting error with deployment time.

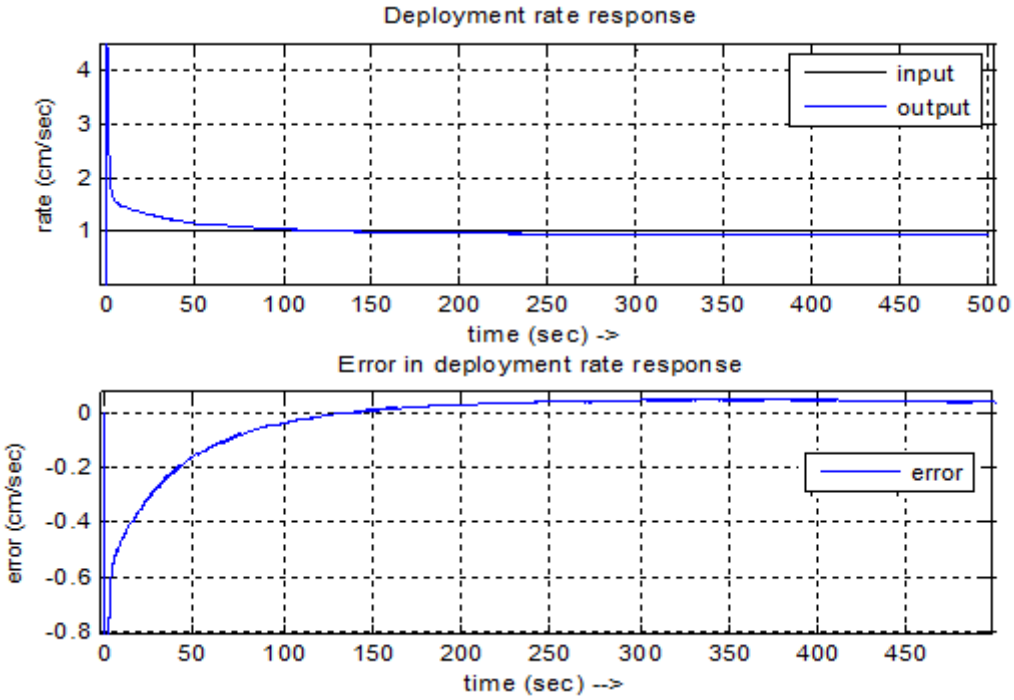

Fig. 4.11: Plot of deployment rate and the resulting error with time.

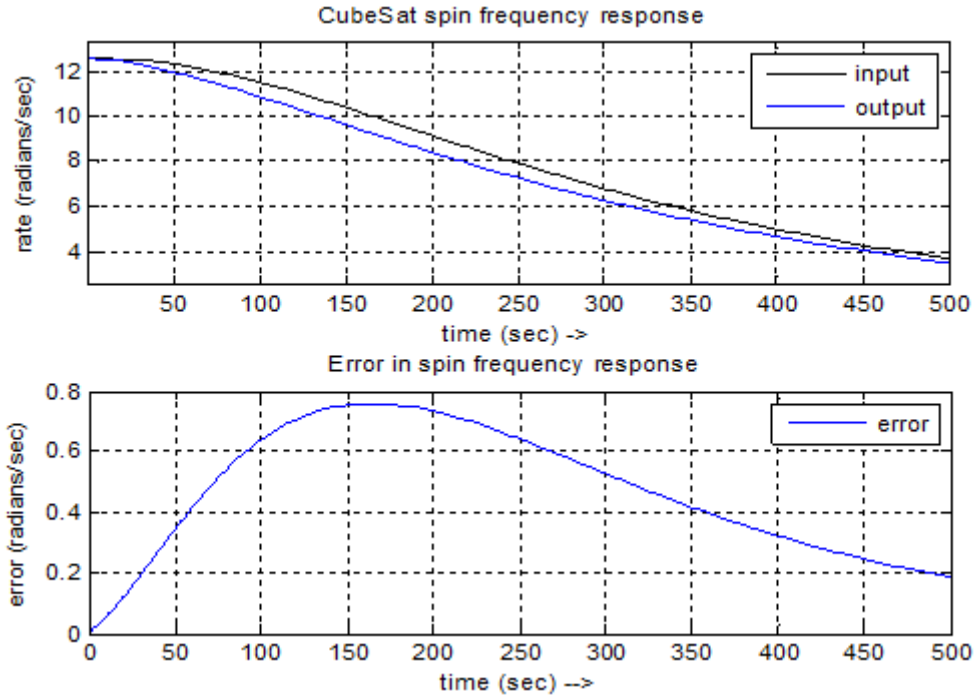

Fig. 4.12: Plot of CubeSat's spin response and the resulting error with time.

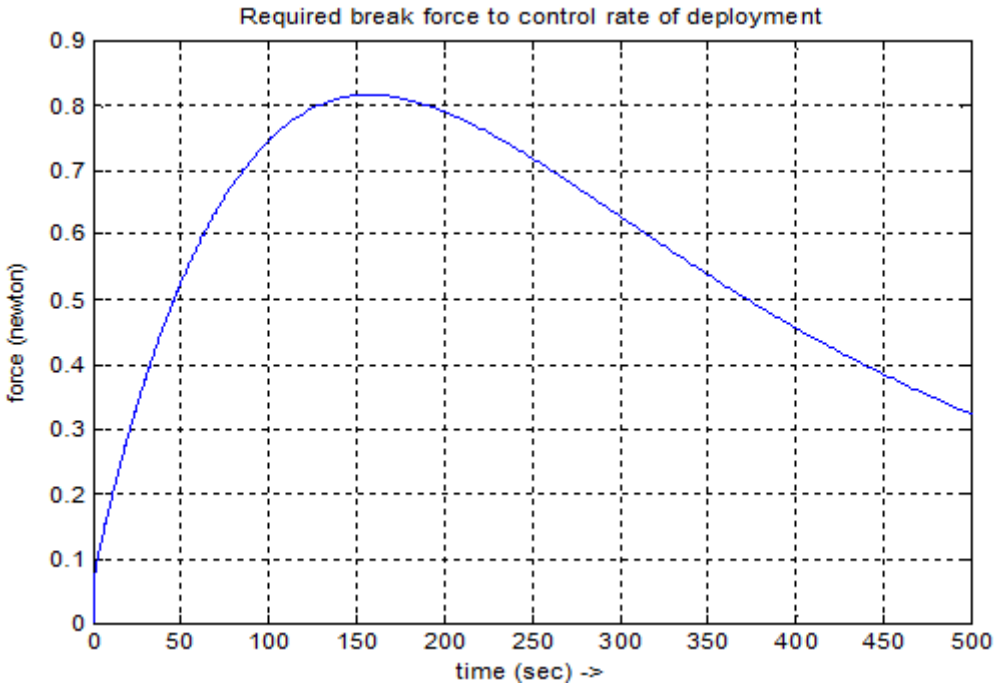

Fig. 4.13: Brake force required to control the rate of wire boom deployment.

Table 4.2: Comparison of controller performance for 2, 3, and 4 Hz as spacecraft's initial spin rate.

CubeSat spin rate when deployment begins (Hz, rads/s)	Boom length (m)	Deployment time duration (s)	Deployment rate peak overshoot (cm/s)	Deployment rate steady state error (%)	CubeSat spin rate after deployment is done (rads/s)	Brake force peak value (N)
Proportional plus Integral Controller Performance						
2, 12.5664	5	500	1.04	1	3.7	0.815
3, 18.8496	5	500	1.09	2	5.58	1.84
4, 25.1327	500	499	1.7	4	7.45	3.26
LQR Controller Performance						
2, 12.5664	5	487	4.5	5	3.72	0.815
3, 18.8496	5	482	9	7	5.59	1.83
4, 25.1327	5	471	16	10	7.45	3.26

value of brake force required to control the deployment rate to 1cm/s increases to about 4 times (3.26 N) from the initial value (.815 N) when spin frequency is increased to twice of its initial value of 2 Hz.

The LQR control system is taking slightly less time than expected. The peak over overshoot is significantly more than that of PI controller. The steady state error is slightly more as compared to the PI controller. The performance of the LQR controller is subject to the weighting factors and there is further possibility of getting slightly better response from the LQR controller by exhaustive tuning of the weighting factors. The LQR control system is designed using the linearized system of dynamics, which may be the reason of inferior control performance. However, linearizing the nonlinear dynamics and then designing a controller and testing it on nonlinear dynamics seems to be a more agreeable way as compared to the hit and trial method to find PI controller gains directly for the nonlinear dynamics.

4.5 Wire Boom Deployment Simulation for Two-Dimensional Model

In this section, simulation results of the two-dimensional dynamics model are presented. The two-dimensional model aims to observe the in-plane deflections of the deploying wire booms. The details of the two-dimensional model were provided in section 2.2.

4.5.1 Fast Deployment Results

The simulation is done for fast deployment scheme to be used for ASSP sub-payloads. As mentioned in section 1.4.2, the sub-payloads need to deploy 2 meters of wire booms in 20 seconds. The wire boom deployment length, velocity, and acceleration plots from fast simulation are shown in Figure 4.14.

In this simulation, the deployment of 2 m wire boom is done is done in 20 seconds, and then no further deployment takes place. The scheme involves acceleration up to 1 m wire boom deployment and then deceleration for another 1 m deployment. The in-plane deflections while wire boom get deployed are shown in Figure 4.15. It also shows the deflection with respect to spinning sub-payload after the deployment is done. Figure 4.16 provides a view of wire boom deflecting (blue) with respect to sub payload(reference line shown in green). Assuming that the value of rotational damping used in ASSP deployment system is $c = 0.00033647$ N-m-sec/rad which is calculated with help of laboratory experiments. The calculation is shown in the Appendix. It can be observed from Figure 4.15 that the magnitude of oscillations while deployment is under 22 degrees and after deployment under 5 degrees, which complies with the requirements mentioned in section 3.1 of Chapter 3.

4.5.2 Slow Deployment Results

The slow deployment involves a deployment rate of 1 cm/s. This simulation results provide insight to in-plane wire boom deflections which may occur while deploying wire boom from DICE CubeSat. Figure 4.17 gives the wire boom deployment profile. The total simulation time is 700 seconds so the deflection occurring after the completion of wire boom deployment may be observed.

The simulation is done for 5 meter wire boom length. In this simulation the velocity is given acceleration of 0.4 m/s to set to a constant value of 1 cm/s from initial zero in a quarter of a second. The inplane deflection are given by Figure 4.18. The wire boom deflections needs to be under 22 degrees according to the requirements given in section 3.1 of Chapter 3.

From Figure 4.18, it is clear that the wire boom's in-plane oscillation is well below 45

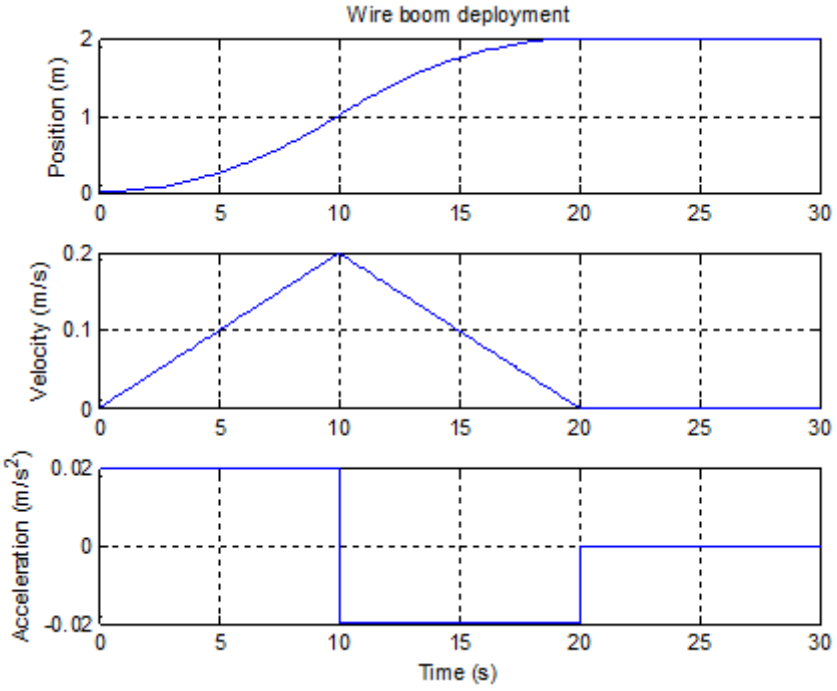

Fig. 4.14: Wire boom deployment profile for fast deployment from ASSP sub-payload.

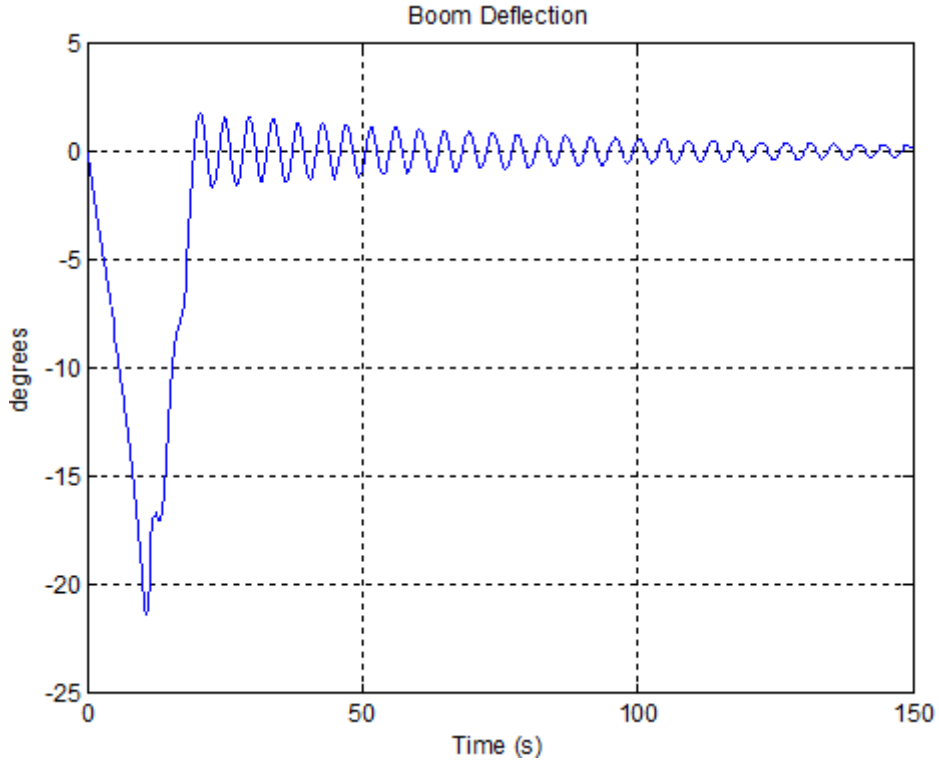

Fig. 4.15: In-plane boom deflection.

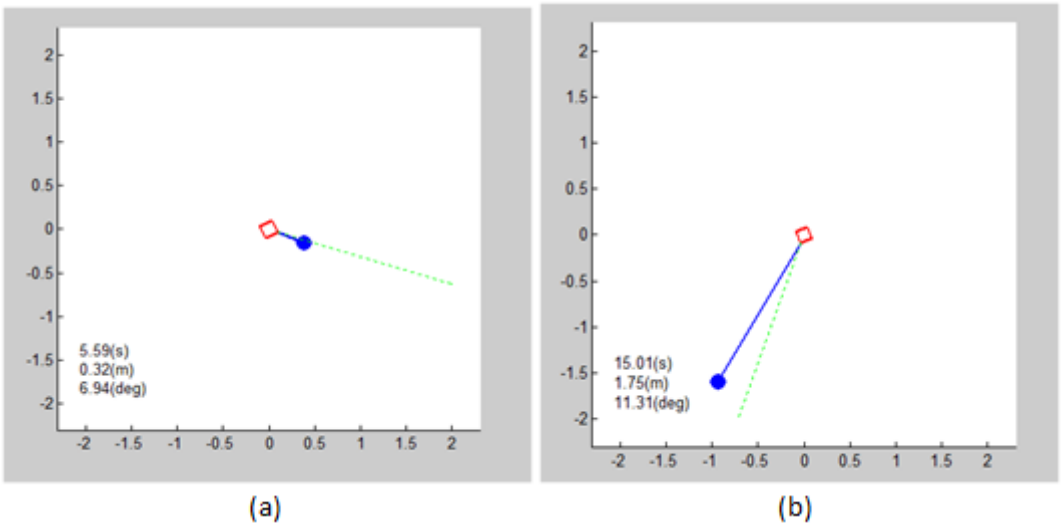

Fig. 4.16: In-plane boom deflection with wire boom deflecting along reference line.

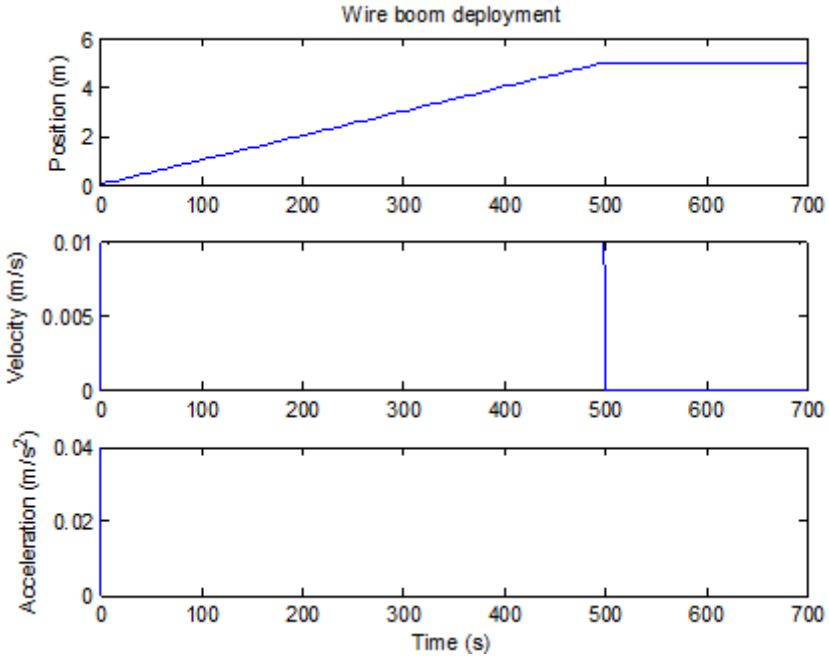

Fig. 4.17: Wire boom deployment profile for slow deployment from DICE CubeSat.

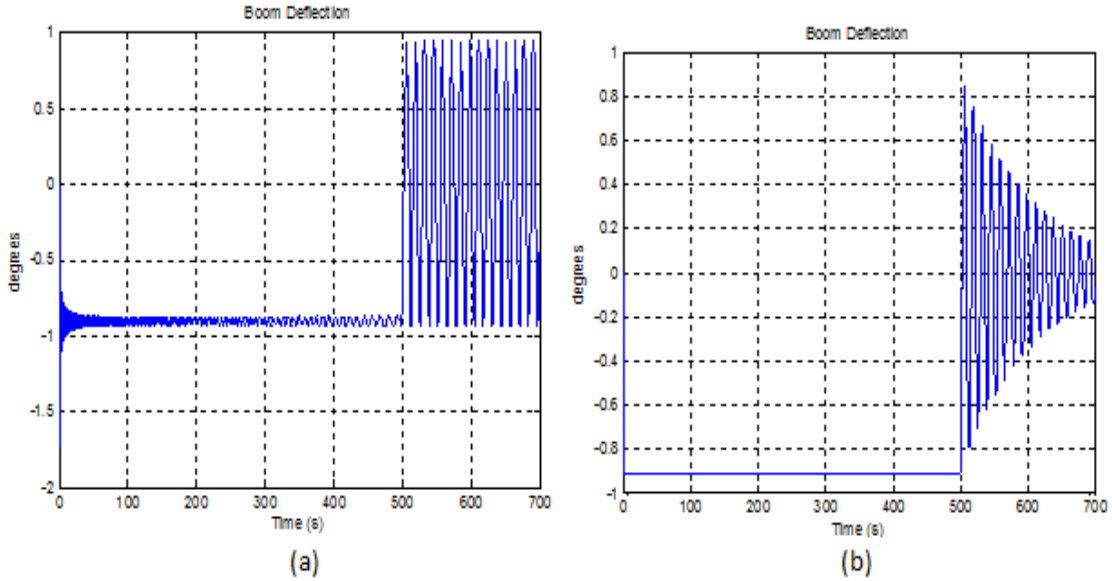

Fig. 4.18: In-plane boom deflections (a) without damping, and (b) with damping.

degrees, which complies with the deployment requirements mentioned in section 3.1. The oscillations will gradually decrease with time due to energy losses in the system such as heat. There is no device installed on DICE CubeSats for significant energy loss or damping, therefore it is not modeled in the deployment dynamics. Since the mission time is far greater than ASSP, there will be enough time available for the oscillation to settle down and proper functioning of the EFP instruments. However, if damping device similar to ASSP is installed on DICE CubeSats, then the oscillations can be suppressed as shown in Figure 4.18(b).

Chapter 5

Conclusion

Wire boom-based electric field measuring instruments are very important to space weather research. Wire boom systems are comparatively light weight and can be deployed with fast or slow deployment rates depending on what mission requirements are. Wire boom-based sensor deployment systems are highly suitable for small spacecrafts such as CubeSat used in DICE Mission or sub-orbital payloads to be used in ASSP Mission. The wire boom-based sensor deployment systems are expected to play an important role in small spacecraft science missions to advance geo-space and atmospheric research funded by National Science Foundation (NSF), and National Aeronautics and Space Administration (NASA). A brief detail about recent small spacecraft missions including already flown DICE as well as proposed ASSP mission was presented in Chapter 1 along with their mission sequences and wire boom deployment schemes. Safe and stable deployment of the wire booms from spacecrafts necessitates controlled deployment operation which in turn requires understanding the involved dynamics. Chapter 2 presented two dynamics models for deploying wire boom from spinning spacecrafts. The first was a simple model where the in-plane deflection of the wire booms and the mass of wire was neglected. It modeled the motion of the tip mass or the spherical sensors attached to the wire booms extending out of the spinning CubeSat. The second model included the in-plane deflection of the wire booms but like the first model ignored the mass of the wire attached to the spherical sensors. The differential equations derived for the first model were then used to develop a control system with proportional plus integral compensator as well as linear quadratic regulator to control the rate of wire boom deployment. The steps involved in the development of the controller were presented in Chapter 3. From the simulation results of the control system presented in Chapter 4, it was found the performance of the PI controller

was slightly better than the LQR controller. The reason behind would be that the LQR controller was developed using linearized dynamics which ignores the nonlinearities found in the motion of wire booms. However, the performance of LQR controller can be further improved by an exhaustive treatment to weighting factors, Q and R. In Chapter 4, we also presented the simulation results of the second model showing the in-plane deflection of the wire booms. Three deployment rate schemes were tested, first two for ASSP mission requiring 2 m boom deployment in 20 seconds, and then the third for the DICE mission deploying 5 m boom in 500 seconds. It was found that the in-plane deflection for first two cases were under the safety norm of 5 degrees. In case of DICE it shows that the magnitude of the deflection is significantly less than 22 degree and can be assumed to be safe. The oscillations may be further suppressed by applying damping similar to one used in case of ASSP sub-orbital payloads. The magnitude of oscillations is shown to be bound by involving an energy damping device like viscous damper in the wire boom deployment assembly. The future work involves development of more advanced dynamics models involving out of plane oscillation of wire booms as well as the mass of the wires. This will enable the development of a model which can closely depict the dynamics occurring in reality. Next step will be to design control system for this more advanced model using the steps already shown in this report to control the rate of the deployment.

References

[1] H. Heidt, J. Puig-Suari, A. S. Moore, S. Nakasuka, and R. J. Twiggs, "Cubesat: A new generation of picosatellite for education and industry low-cost space experiments," in *Proceedings of AIAA/Utah State University Conference on Small Satellites*, Aug. 2000.

[2] "Cubesat-based science missions for space weather and atmospheric research program solicitation nsf 08-549," *The National Science Foundation*, 2006, accessed 5 May 2012. [Online]. Available: http://www.nsf.gov/pubs/2008/nsf08549/nsf08549.htm.

[3] M. L. Psiaki, P. M. Kintner, and S. P. Powell, "Rapid energy dissipation in a yo- yo-type wire boom deployment system," *Journal of Guidance, Control, and Dynamics*, vol. 23, no. 3, May-June 2000.

[4] V. M. Pillet, A. Aparicio, and F. Sanchez, *Payload and Mission Definition in Space Sciences*. Cambridge University Press, ch. 7, pp. 252–253, 2005.

[5] P. Pakdeepattarakorn, P. Thamvechvitee, J. Songsiri, M. Wongsaisuwan, and D. Banjerdpongchai, "Dynamic models of a rotary double inverted pendulum system," in *Proceedings of IEEE Region 10 Conference*, pp. 558 – 561, Nov. 2004.

[6] J. W. Bonnell, F. S. Mozer, G. T. Delory, A. J. Hull, R. E. Ergun, C. M. Cully, V. Angelopoulos, and P. R. Harvey, "The electric field instrument (efi) for themis," *Space Science Reviews*, vol. 141, 2008.

[7] P. David, B. Robert, W. Robert, and U. Robert, "Deployment mechanisms on the fast satellite: Magnetometer, radial wire, and axial booms," *Space Science Reviews*, vol. 98, 2001.

[8] J. F. G. Lodoso, J. J. Echevarria, and J. M. Gavira, "Wire boom mechanism for bepicolombo mission to mercury," in *9th European Space Mechanisms and Tribology Symposium*, vol. D, pp. 171–178. ESA Publications Division, 19-21 September 2001.

[9] L. Blomberg, H. Matsumoto, J.-L. Bougeret, H. Kojima, S. Yagitani, J. Cumnock, A. Eriksson, G. Marklund, J.-E. Wahlund, L. Bylander, L. hln, J. Holtet, K. Ishisaka, E. Kallio, Y. Kasaba, A. Matsuoka, M. Moncuquet, K. Mursula, Y. Omura, and J. Trotignon, "Mefisto an electric field instrument for bepicolombo/mmo," *Advances in Space Research*, vol. 38, no. 4, pp. 672 – 679, 2006. [Online]. Available: http://www.sciencedirect.com/science/article/pii/S0273117705006265.

[10] M. Psiaki, S. Powell, E. Klatt, and J. P.M. Kintner, "Practical design and flight test of a yo-yo wire boom deployment system," *Journal of Guidance, Control, and Dynamics*, vol. 28, no. 1, Jan.-Feb. 2005.

[11] G. Crowley, C. Fish, C. Swenson, R. Burt, E. Stromberg, T. Nielson, S. Burr, A. Barjatya, G. Bust, and M. Larsen, "Dynamic ionosphere cubesat experiment (dice)," in *Proceedings of AIAA/Utah State University Conference on Small Satellites*, Aug. 2011.

[12] S. Grover, K. Bradford, M. Anderson, E. Stromberg, B. Sharp, and S. Burr, "Miniature wire boom system for nano satellites," in *Proceedings of AIAA/Utah State University Conference on Small Satellites*, Aug. 2010.

[13] S. T. Lai, H. Mahon, and M. Smiddy, "Dynamics of wire boom oscillations on a spinning satellite part i, lagrangian equations of motion and transient response," *Zeitschrift fr Angewandte Mathematik und Physik (ZAMP)*, vol. 30, pp. 1–11, 1979, 10.1007/BF01597476. [Online]. Available: http://dx.doi.org/10.1007/BF01597476.

[14] "Double pendulum," *Eric Weisstein's World of Science*, 2007, accessed 10 December 2011. [Online]. Available: http://scienceworld.wolfram.com/physics/DoublePendulum.html.

[15] I. Nagarath and M. Gopal, *Control Systems Engineering.* New Age International (P) Limited Publishers, ch. 4, pp. 417–453, 2004.

[16] N. S. Nise, *Control Systems Engineering.* New Delhi: John Wiley and Sons, ch. 9, pp. 439–449, International Student Version, 2010.

[17] J. Watkins and E. Mitchell, "A matlab graphical user interface for linear quadratic control design," in *Frontiers in Education Conference, 30th Annual*, vol. 2, pp. F4E/7 –F4E10, 2000.

Appendix

Appendix A

Coefficient of Rotational Damping

A.1 Calculation of Coefficient of Roational Damping

This section shows how the value of coefficient of roational damping was calculated, to be further used in two-dimensional dynamics model simulations. The value of coefficient of rotational damping can be calculated by comparing the standard second order differential equation of damped oscilaator with the equation of motion of the pendulum setup used in experiments for ASSP sub-payloads in the Space Dynamics Lab.

The second order differential equation for a damped oscillator is given by the famous expression

$$\ddot{\theta} + \frac{\omega_o}{Q}\dot{\theta} + \omega_0^2\theta = 0, \tag{A.1}$$

where Q is the quality factor for the oscillator. For systems with fairly small damping, Q is defined as

$$Q = 2\pi\frac{E}{|\Delta E|}, \tag{A.2}$$

where E is the energy of oscillation and ΔE is the energy lost per cycle because of dissipation. The dissipation is commonly expressed in terms of either the damping ratio, ζ, or expressed in terms of an attenuation factor β.

$$\zeta = \frac{1}{2Q} = \frac{\beta}{\omega_0} \tag{A.3}$$

Thus, the classic damped oscillator equation is written as

$$\ddot{\theta} + 2\zeta\omega_0\dot{\theta} + \omega_0^2\theta = 0, \tag{A.4}$$

or

$$\ddot{\theta} + 2\beta\dot{\theta} + \omega_0^2\theta = 0. \tag{A.5}$$

The equation of pendulum motion setup used in the experiment is

$$ml^2\ddot{\theta} + c\dot{\theta} + mglsin\theta + k\theta = 0, \tag{A.6}$$

where c is coefficient of roational damping with units N-m-sec/rad and k is coefficient of torsion spring with units N-m/rad,

$$\ddot{\theta} + \frac{c}{ml^2}\ \dot{\theta} + \frac{mgl}{ml^2}\ sin\theta + \frac{k}{ml^2}\theta = 0, \tag{A.7}$$

for small angle, $sin\theta \approx \theta$

$$\ddot{\theta} + \frac{c}{ml^2}\ \dot{\theta} + \frac{g}{l}\ \theta + \frac{k}{ml^2}\theta = 0, \tag{A.8}$$

ignoring the term with k

$$\ddot{\theta} + \frac{c}{ml^2}\dot{\theta} + \frac{g}{l} = 0, \tag{A.9}$$

comparing with

$$\ddot{\theta} + \frac{\omega_o}{Q}\dot{\theta} + \omega^2{}_o\theta = 0, \tag{A.10}$$

hence

$$\frac{c}{ml^2} = \frac{\omega_o}{Q}, \tag{A.11}$$

or

$$c = \frac{\omega_o ml^2}{Q}, \tag{A.12}$$

similarly

$$\omega_o = \sqrt{\frac{g}{l}}, \tag{A.13}$$

also

$$\zeta = \frac{1}{2Q}\ or\ Q = \frac{1}{2\zeta}, \tag{A.14}$$

then

$$c = 2\omega_o m l^2 \zeta. \tag{A.15}$$

For ASSP sub-payload the structural parameters are

$m = 10\ g$, mass of bob;

$g = 9.8\ m/s^2$, aceleration due to gravity;

$l = 2\ m$, length of pendulum;

ζ=.0019, damping constant (in vacuum as per test results).

The value of c calculated with equation (A.15) is

$$c = 0.00033647 \text{ N-m-sec/rad.} \tag{A.16}$$

A.2 Methodology Used in Damping Tests

The damping tests were run in two different environments, first in air and second in a vacuum. Several tests were conducted within each test environment varying parameters for each test case. The parameter that was be varied is the length of the wire. The test setup consisted of the same hardware being used on DICE, i.e., corner mounts, wire, and guide rail. The damping washer used in the test is likely be the same or similar to one that will be used in ASSP sub-payloads. For tracking the motion of the wire boom pendulum photo interrupt sensors were used. The setup consisted of two photo interrupt sensors to track the period of the motion as well as the velocity. The sensors were interfaced with Matlab and the data was logged along with the test time. The value of ζ= .0019 used in previous section to calculate the coefficient of roational damping c used for simulations in this report was taken from the test done in vacuum environment. Equation (A.15) shows that the value of c is dependent on length of the pendulum l given in $meters$, mass of bob or sphere m given in $grams$, damping ratio ζ and natural frequency ω_o given in rad/s. The length of wire used in the test setup was .37456 $meters$ and the mass of sensor sphere was 1.23 $grams$.

Figure A.1 shows the decay in oscillation amplitude in a test done in vacuum environment. Figure A.2 shows the variation in the value of damping ratio ζ measured in the test.

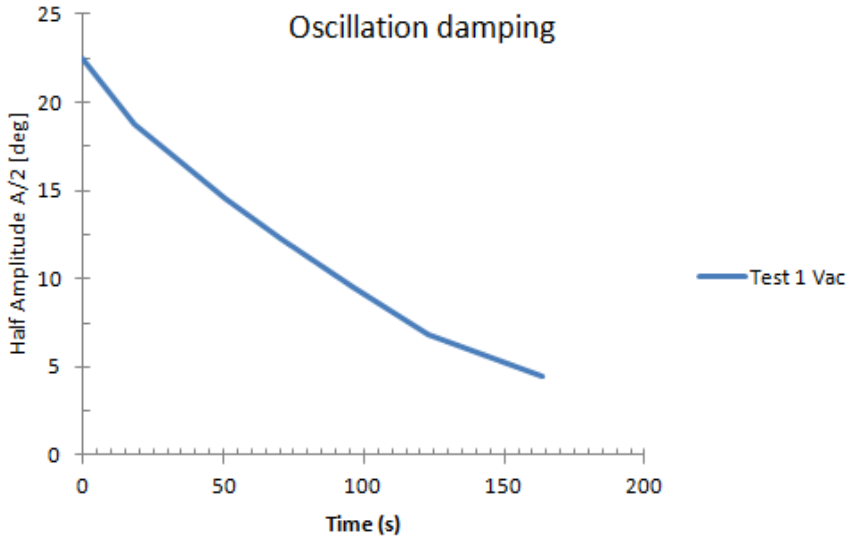

Fig. A.1: Decrease in oscillation amplitude with time.

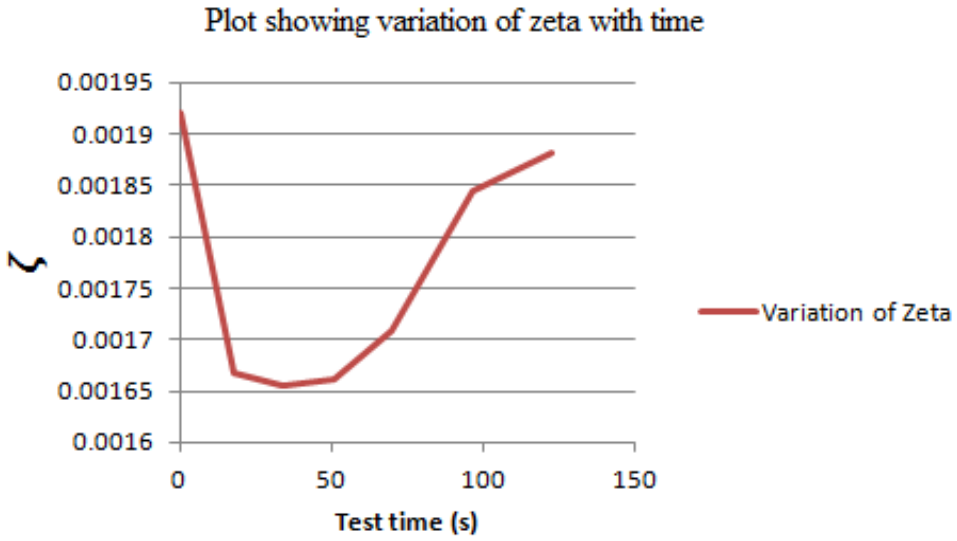

Fig. A.2: Variation in the value of ζ with time.